SUM4Re

Creating materials banks
from digital urban mining

D2.6 FOS methodological framework acquisition

VERSION 1.0

PUBLIC

28 October 2025

Associated with document Ref. 101129961

Funded by the European Union. Views and opinions expressed are however those of the author(s) only and do not necessarily reflect those of the European Union. Neither the European Union nor the granting authority can be held responsible for them.

Funded by the European Union

SUM4Re

Creating materials banks from digital urban mining

Deliverable ID	D2.6
Deliverable name	FOS methodological framework acquisition
Lead partner	TECN
Contributors	MOYUA

PUBLIC

Funded by the European Union

DOCUMENT INFORMATION

Document name	D2.6 FOS methodological framework acquisition
Version	1.0
Due date	31/10/2025
Report date	27/10/2025
Number of pages	51
Lead Author	Jose Carlos Jimenez Fernandez (TECN)
Other Authors	-
Dissemination level	Public

REVISION HISTORY

Rev.	Date	Description of revision
0.1	24/03/2025	Initial version
0.2	01/10/2025	First draft version
0.3	14/10/2025	Revised draft version
1.0	27/10/2025	Final version (approved)

DOCUMENT APPROVAL

Written	Jose Carlos Jimenez Fernandez (TECN)	01/10/2025
Revised	Giovanni Scilipoti (SINTEF), Tom Lacroix (BLOCKM)	14/10/2025
	Ana Sánchez (UVIGO, Project Manager)	27/10/2025
Approved	Pedro Arias Sánchez (UVIGO, Project Coordinator)	27/10/2025

EXECUTIVE SUMMARY

Deliverable D2.6 (Task 2.6) reports on the development, validation, and integration of a fibre optic sensor (FOS)-based framework for structural health monitoring (SHM) of reusable steel elements. The work combines high-resolution strain and vibration sensing, finite element model FEM inverse calibration algorithms, and AI-based damage identification. It is central to Work Package WP2, as it establishes the methodologies and datasets required to support transfer learning approaches in WP3 and pilot demonstrations in WP10.

The first phase of the work focused on the identification and instrumentation of target structures. An I-profile steel beam, originally used to support an overhead crane in an industrial building from the 1950s, was selected due to its manageable size, ease of handling for reuse, moderate section properties (facilitating static testing without heavy loading equipment), and the availability of multiple similar beams for future transfer learning applications. A preliminary visual inspection confirmed no apparent damage, ensuring suitability for testing.

The second phase consisted of the experimental campaign, carried out in collaboration with MOYUA. Fibre Bragg grating (FBG) strain sensors (FS62) and optical accelerometers (FS65) were installed and interrogated using the QuantumX MXFS unit. Static loading tests provided strain–displacement relationships, while dynamic excitation enabled modal identification through FFT-based analysis. The testing demonstrated the feasibility of multiplexed FOS installations, which offered reduced installation effort, high-resolution data, and robustness in harsh environments compared with conventional gauges.

The third phase addressed the FEM calibration. Initial comparisons revealed a strong discrepancy between static and dynamic estimates of Young's modulus due to non-ideal boundary conditions. By refining the support modelling to account for partial fixity and cantilever effects, a compromise modulus of ≈155 GPa was identified through a combined RMSE–MAE minimisation. This value, consistent with typical steels used in the Basque Country in the 1950s, ensures balanced performance in both static and dynamic simulations. Importantly, this calibrated modulus will serve as the baseline for generating synthetic datasets of damaged and boundary condition scenarios, which will be used to train transfer learning algorithms in Task 3.6 (WP3).

The fourth phase developed a damage identification framework, combining global indicators (frequency shifts from operational modal analysis) and local indicators (strain distribution tendencies from FOS). By training anomaly detection models on FEM-simulated healthy states, deviations in either frequency content or strain profiles can be flagged as potential

damage. This dual-indicator approach increases robustness and paves the way for scalable application across multiple structural typologies.

The deliverable also highlights challenges and limitations, including sensor bonding quality, environmental effects on signals, computational cost of FEM calibration, and the need for larger, more representative datasets. Mitigation strategies include improved installation protocols, temperature compensation, more efficient optimisation routines, and the generation of synthetic datasets for AI model training.

In conclusion, Deliverable D2.6 provides a validated methodological framework for FOS-based SHM, integrating sensing, modelling, and AI. The results demonstrate the feasibility of applying FOS for reusable structural components, with direct implications for digital twins, circular-BIM integration, and digital product passports. The outputs of this work form a crucial bridge to WP3, where transfer learning and anomaly detection will be further developed, and to WP10, where real-world pilot testing will validate the approach under operational conditions.

GLOSSARY

Terms, Abbreviations, and Acronyms

AI	Artificial Intelligence
BIM	Building Information Modelling
C-BIM	Circular-BIM
EC	European Commission
EU	European Union
GDPR	General Data Protection Regulation
SUM4Re	Creating material banks from digital urban mining (project name)
WP	Work Package
WA	Work Area
RMSE	Root mean square error
MAE	Medium average error
FOS	Fiber optic sensor
FFT	Fast Fourier Transform
SHM	Structural Health Monitoring
GPa	Giga Pascal (unit)
UN	United Nations
DAS	Distributed Acoustic Sensing
DPPs	Digital Product Passports
OMA	Operational Modal Analysis

TABLE OF CONTENTS

LIST OF TABLES

LIST OF FIGURES

1. Introduction

This delivery service serves to describe the progress made and results achieved for Task 2.6:

T2.6 Structural health monitoring system with FOS(M3-M17) TECN; MOYUA

This task will provide an integrated structural health monitoring system, whose main steps are: (1) Identification of target structures; (2) Definition of a Risk-based assessment framework; (3) Creation of predicted responses based on pool of local models; (4) Selection of appropriate FOS sensors to capture the actual structural response (e.g., accelerations, deformations, etc.) and other variables (e.g. temperature, humidity, etc.); (5) Installation and inverse-modelling for calibration of the system; and (6) Damage identification applying AI-techniques (e.g. Neural Networks) to the collected structural response data. This task will demonstrate the added value of FOS: higher measurement quality, higher reliability, easier installation/deinstallation and maintenance, and lower lifetime cost extending the life of the monitored system. FOS will be installed in WP10 in collaboration with MOYUA.

In addition, Task 2.6 is directly related to Task 10.1, since the inverse-modelling and calibration of the FEM model of the monitored structural elements depend on the acquisition of experimental data carried out in the pilot sites. The testing campaigns and data collection activities defined in T10.1 provide the necessary input for validating and adjusting the numerical models developed in T2.6. This interdependency ensures that the FEM calibration is based on real structural responses, thereby increasing the accuracy, robustness and practical relevance of the proposed structural health monitoring system.

2. Research approach

2.1. State of the art

The use of fibre-optic sensors (FOS) for structural health monitoring (SHM) has matured significantly in recent years and is now considered one of the most promising solutions for long-term, reliable and cost-effective monitoring of civil infrastructure. FOS technologies are generally divided into two main families: quasi-point sensors, predominantly Fiber Bragg Gratings (FBGs), and distributed fibre-optic sensing (DFOS) systems, which rely on Rayleigh, Brillouin or Raman scattering and more recently Distributed Acoustic Sensing (DAS). Each of these technologies has specific advantages and trade-offs. FBGs are highly accurate quasi-point sensors capable of multiplexing along a single fibre, which allows dense deployment in locations of interest to measure strain and temperature with very high precision [1]. DFOS solutions, on the other hand, provide continuous measurements along the length of the fibre, enabling a true “digital skin” for structures [2]. Rayleigh-based systems (often using Optical Frequency Domain Reflectometry) provide high spatial resolution at short to medium ranges, whereas Brillouin-based methods offer coverage of tens of kilometres with coarser resolution, ideal for long tunnels, bridges or pipelines. DAS has opened new opportunities for dynamic and acoustic sensing, such as vibration-based monitoring, event detection and ambient modal analysis [3].

These technologies present several strengths compared with traditional electrical sensors. They are immune to electromagnetic interference, allow long-distance transmission of signals without degradation, and can provide either dense or continuous measurements depending on the chosen interrogation method. When combined with appropriate packaging and installation strategies—embedding in concrete, bonding on surfaces, or routing within protective conduits—FOS offer durability and reliability, making them well suited for permanent SHM systems. While interrogator units represent a significant upfront investment, the overall cost of ownership is often lower in long-term monitoring scenarios, as the reduced number of cables, improved durability and multiplexing capabilities simplify maintenance and extend service life [4].

From a monitoring perspective, FOS enable the measurement of multiple variables that are central to structural assessment. Strain, temperature and vibration are the most common, but humidity and other environmental effects can also be indirectly captured through sensor packaging or coatings. As these variables strongly influence structural performance, FOS provide an excellent basis for integrated monitoring systems that support predictive maintenance. However, to translate raw FOS measurements into actionable knowledge, advanced data processing and modelling strategies are required. This is where calibration and inverse modelling play a crucial role. Current state-of-the-art approaches combine high-fidelity finite element models

with optimisation methods, such as genetic algorithms, Bayesian inference or gradient-based solvers, to adjust uncertain parameters so that predicted responses match measured data. This type of model updating reduces uncertainty and enhances the predictive capability of structural digital twins. In distributed sensing applications, inverse modelling is also essential for converting long profiles of strain or temperature into meaningful damage indicators, such as crack opening or local settlements.

A parallel line of development in recent years has been the integration of artificial intelligence (AI) with FOS-based SHM. Machine learning and deep learning techniques are now used for denoising and preprocessing raw FOS signals, for feature extraction such as automated modal analysis, and for damage detection through supervised or unsupervised classifiers. Neural networks, convolutional and recurrent architectures, autoencoders and anomaly detection algorithms have all been applied successfully to structural monitoring datasets [5]. Transfer learning and domain adaptation are increasingly investigated to bridge the gap between laboratory-trained models or FEM simulations and field conditions, which are inherently noisier and subject to environmental variability such as temperature and humidity [6]. Hybrid approaches that combine physical constraints with data-driven models are particularly promising, as they enhance interpretability and reduce false alarms, a major barrier to adoption in the field.

At the system level, modern SHM is moving toward risk-based assessment frameworks that integrate sensor measurements, predictive models and consequence analysis. In these frameworks, FOS data are not used in isolation but are embedded within probabilistic models that account for structural fragility, loading scenarios and the cost of failure. This allows prioritisation of interventions and condition-based maintenance strategies, directly supporting asset life extension. Uncertainty quantification is central to these approaches, ensuring that decision-makers receive not only predictions but also confidence levels that guide risk management. By adopting this perspective, SHM moves from simple damage detection to a more holistic decision-support tool.

Case studies in Europe and beyond have demonstrated the viability of FOS for bridges, tunnels, pipelines and other critical assets, confirming the technology's added value in terms of higher measurement quality, greater reliability, easier installation and deinstallation, and lower lifetime costs compared with traditional sensing networks. Nevertheless, several challenges remain. These include improving field-robust domain adaptation for AI models, standardising installation and calibration protocols, and refining methods for converting distributed measurements into engineering-level damage metrics. Ongoing European initiatives such as SUM4Re show that the integration of advanced sensing, inverse modelling and digital asset management is a priority for both research and practice, and the task at hand is positioned within this frontier.

2.2. Relevance to the WP2 objectives

Against this background, the task foreseen in the project directly addresses the main gaps of the current state of the art by proposing an integrated SHM system with six main steps: identification of target structures, definition of a risk-based assessment framework, creation of predicted responses from a pool of local models, selection of appropriate FOS technologies to capture structural and environmental variables, installation and calibration through inverse modelling, and finally damage identification via AI-based techniques. The demonstration of this workflow in collaboration with MOYUA will provide practical evidence of the benefits of FOS for infrastructure monitoring, while also delivering replicable protocols for calibration, model updating and AI-driven diagnosis. By doing so, the task will showcase the added value of FOS in extending the life of monitored systems and reducing overall costs, while maintaining or even improving safety and reliability standards.

2.3. Relevance to the other WP objectives

Task 2.6 is mainly related to:

- **WP3**: Specifically, T3.6, where long-term monitoring data from FOS will support transfer learning and anomaly detection methods, and T3.7, where this data will be integrated in GENIA.
- **WP6**: T2.6 serves as the structural health information base to propose Circular-BIM (C-BIM) designs but will also be the modelling basis for all data integration (from other sensors and Tasks 2.x) into GENIA and the materials platforms CIRDAX and CONCULAR.
- **WP10**: The methodology and the software developed in T2.6 are necessary for data acquisition in the Spanish case study.

2.4. Legal considerations

The deployment of fibre optic sensors (FOS) for structural health monitoring in the SUM4Re framework must comply with European and national regulations governing construction, monitoring, and occupational safety. At the European level, the Construction Products Regulation (EU) No 305/2011 [7] and related standards (e.g. Eurocodes for structural assessment) provide the reference framework for performance-based evaluation of civil structures. The monitoring activities undertaken in Task 2.6 are consistent with these standards, as they are non-destructive and focused on structural performance parameters (strain, vibration, stiffness degradation).

In Spain, specific compliance is required with the *Código Técnico de la Edificación (CTE)* [8] and *Instrucción de Acero Estructural (EAE)* [9], which define safety margins, durability, and verification requirements for steel structures. The FOS instrumentation does not interfere with structural

integrity and thus remains within the scope of accepted non-invasive diagnostic methods. Additionally, the experimental campaign followed occupational risk prevention guidelines (*Ley 31/1995 de Prevención de Riesgos Laborales*) [10], ensuring that installation and testing were conducted under safe working conditions.

From a data governance perspective, the measurements acquired form part of the SUM4Re database and must comply with FAIR data principles and the project's Data Management Plan (DMP). Intellectual property generated by calibration algorithms and AI workflows will be managed under the consortium agreement, while raw sensor data will be anonymised and stored according to GDPR requirements when linked to pilot-site stakeholders.

2.5. Target materials

The monitoring campaign of Task 2.6 is focused on structural steel elements, as they represent a critical material in the Spanish pilot. Steel beams are widely used in temporary and permanent structures and are directly linked to the project's circular economy objectives, since they can be dismantled, reconditioned and reemployed with minimal loss of mechanical performance.

By focusing on steel beams, the deliverable provides direct evidence of how FOS can support multi-life cycle assessments of structural materials, generating traceable data that can be integrated into Digital Product Passports (DPPs) and Circular-BIM workflows.

2.6. Case studies application

The Spanish pilot case is the primary application context for Task 2.6. In collaboration with MOYUA, a series of steel beams were instrumented with fibre optic sensors to demonstrate the feasibility of SHM for reusable components. The sensors were bonded directly to the steel surface and interrogated using a QuantumX MXFS unit, enabling high-resolution acquisition of strain and vibration data during both static and dynamic testing.

This case study is an abandoned industrial factory in Jolastokieta, Spain. This building is mostly empty, and structural elements are the only remains. It features some thin metal beams and columns that aided the machinery. The floor, ceiling and walls are made of stone, metal and concrete, respectively. An indoors picture can be seen in Figure 1. Further details can be consulted on Deliverable D10.1.

Figure 1. Spanish case study (Jolastokieta)

Two main test campaigns were executed:

- Static loading tests – beams were subjected to incremental loads to capture full strain distributions, identify stiffness characteristics, and validate FEM-based calibration with genetic algorithms.
- Dynamic excitation tests – beams were excited through controlled impacts to extract modal frequencies and damping ratios, enabling comparison with numerical predictions and assessment of degradation under reuse cycles.

The results confirmed that FOS provide reliable, multiplexed strain and vibration data with reduced installation times compared to conventional gauges. More importantly, the monitoring demonstrated that structural steel beams retain predictable behaviour across repeated load cycles, validating their potential for safe reuse in secondary applications.

This case study establishes a methodological blueprint for extending FOS-based SHM to other materials and pilots within SUM4Re, but in D2.6 the focus remains on the Spanish steel beam monitoring campaign as a proof-of-concept for circular structural assessment.

3. Technical brief

This section provides a detailed overview of the fibre optic sensing (FOS) system deployed within Task 2.6 of the SUM4Re project, with emphasis on its technical specifications, sampling strategies, and practical implementation in the Spanish pilot case. The objective is to establish a clear framework for the use of FOS in structural health monitoring (SHM), focusing on steel elements representative of reusable structural components.

The application of FOS in this context is motivated by several advantages over conventional electrical sensors. Fibre Bragg grating (FBG)-based systems enable high-resolution strain and vibration measurements, immunity to electromagnetic interference, and the multiplexing of numerous sensing points along a single optical fibre. These characteristics make FOS particularly well suited for continuous, long-term monitoring in harsh or variable environments, as encountered in abandoned or rehabilitated building structures.

3.1. Equipment description with respect to application and utilization

3.1.1. Properties of the FOS

The fibre optic sensing (FOS) system deployed in this task is based on HBM newLight sensors [11] coupled with the QuantumX MXFS optical interrogator. These sensors rely on fibre Bragg grating (FBG) technology, which provides precise strain, vibration, and temperature measurements along optical fibres.

Table 1 summarizes the main technical details of both deformation sensors (FS62) and vibration sensors (FS65).

Table 1. Properties of the FOS sensors

Sensor	Type	Capabilities	Key Properties
newLight FS62 / FS62CSS	Deformation / Strain sensor (FBG)	Precise, stable strain measurement. Exact numerical strain range isn't shown in the Spanish page due to internal error, but generally, FBG strain sensors are capable of micro-strain resolution and large dynamic range. *newLight* line promises high long-term stability.	Uses fibre Bragg grating (FBG) technology. Robust construction, resistant to humidity, corrosion, salty environments. Offers stability and repeatability over long periods.
newLight FS65	Optical accelerometer (vibration)	Measures accelerations up to ±10 g, at low frequency range (0-50 Hz).	FBG-based accelerometer, so optical and passive (no electrical signals at sensing head). IP68 protection, safe in harsh environmental conditions (humidity, salinity). Linearity < 2% over the measurement range. Can be used in monoaxial mode; multiple sensors allow multi-axis measurement.

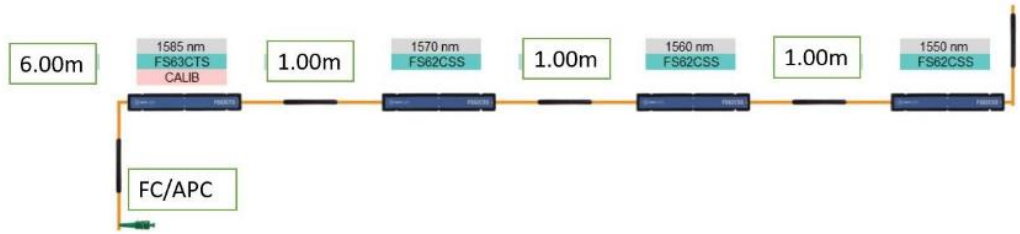

Figure 2. FOS array designed for SUM4Re testing

Table 2 summarizes the main technical specifications of the FOS employed in this research.

Table 2. Technical specifications of the FOS

FS62-CSS	***FS65ACC***
Gauge length: 10 mm Measurement range: ±5,000 με Accuracy: ±1 με Resolution: <0.1 με Temperature compensation: Integrated FBG-based Connector type: Optical FC/APC Packaging: Stainless steel encapsulated	Measurement range: ±5 g Frequency range: DC to 3,000 Hz Resolution: <0.01 g Sensitivity: 80 pm/g Operating temperature: −40 °C to +80 °C Measurement axes: Triaxial

Following the sensors description, it is highlighted the optical interrogator properties (QuantumX MXFS). The QuantumX MXFS module acts as the interface between FBG sensors and the digital acquisition system. Its technical features include:

- Channel capacity: Up to 8 optical connectors, each supporting up to 16 FBG sensors, resulting in a maximum of 128 simultaneous channels per module.
- Sampling rates:
  - Normal speed mode: up to 100 samples per second per channel, suitable for long-term monitoring of slow changes such as creep or temperature drift.
  - High-speed mode: up to 2,000 samples per second per channel, suitable for dynamic monitoring such as vibration and transient loads.
- Measurement types supported: Strain, temperature, acceleration, load, and tilt, depending on the sensor configuration.
- Accuracy and resolution: Wavelength measurement resolution of a few picometers, corresponding to high sensitivity in strain and temperature readings.
- Integration and interfacing: Fully compatible with catman® software (v5.4 or higher) for real-time visualisation, analysis, and reporting. It also allows synchronisation with other

QuantumX modules, enabling hybrid optical/electrical acquisition and open interfaces with LabVIEW and APIs.

Figure 3. QuantumX optic interrogator

3.1.2. Other equipment

Apart from the FOS equipment, it was used load cells for measuring and controlling the load applied onto the testing specimens. The Utilcell Modelo 620 is a traction-compression load cell used to measure forces (load) applied in both tension and compression. It is well suited for static and quasi-static structural testing where accuracy, environmental resistance, and a good range of capacities are required. Table 3 presents the main technical specifications.

Table 3. Technical specifications of the load cells

Parameter	Specification / Detail
Device type	Traction-Compression load cell (strain gauge based)
Model	Utilcell Modelo 620
Capacity / Measurement ranges	Available in multiple ranges: 50, 100, 150, 200, 300, 500, 750, 1 000, 1 500, 2 000, 3 000, 5 000 and 6 000 kg (i.e. approximately up to ~60 kN for 6 000 kg).
Material / Mechanical structure	Elastic support made of alloy steel.
Protection / Environmental rating	IP67 rating (dust-tight, protected against immersion up to depth/time specified).
Accuracy / Divisions	3 000 divisions (OIML R60, Class C)
Corrosion resistance	Hard-nickel (níquel duro) anticorrosion treatment.
Typical applications	Tanks, hoppers, weighing suspended structures, asphalt and concrete plants, machinery testing, aerial weighing. Useful in static test rigs for applied loads.
Accessories / Mechanical fittings	Available with thread/connection accessories: TE12×1.75, TE16×2, TE24×2 for lower capacities; RO12×1.75, RO16×2, RO24×2 for medium-to-higher capacities. These ensure compatibility with the mechanical mounting in test setups.

3.2. Sampling methods

3.2.1. Expected output data and measurements needed

- Strain profiles along structural elements (FS62) with high resolution and low drift over time.
- Vibration signatures and acceleration data (FS65) especially for low frequency phenomena (0-50 Hz), for example vibrations induced by traffic, occupancy loads, or nearby construction.
- Temperature compensation or measurements to correct strain readings (for those sensors that include dual FBGs for temperature).
- Time series data for static testing are synchronized with load cell measurements, to link the load applied with the deformation response.

3.2.2. Preparatory measures

Daily activities in the building that must be considered

Since the selected pilot building is abandoned and not in active use, there are no daily operations, occupants, or ongoing activities that need to be coordinated with during FOS installation and monitoring. This eliminates potential interferences such as vibrations from occupancy, accessibility restrictions, or scheduling conflicts with users. However, the absence of maintenance or active services also requires additional planning for power supply, security, and safe access to the site.

Location of the FOS activities

All FOS acquisition activities will take place inside the building, with priority given to structural elements representative of the building's load-bearing system. The indoor location ensures protection from direct environmental exposure, although humidity, dust, and debris typical of abandoned structures must be considered when preparing surfaces and protecting optical fibres.

3.2.3. Practical and technical requirements

- Mounting and orientation: FS62 sensors must be bonded or affixed along the axis of expected strain (beam, slab, joint). Adequate surface preparation needed to ensure adhesion and accurate reading. For FS65 accelerometers, orientation relative to expected vibration vector matters (monoaxial or multi-axis). Multiple sensors may be needed to capture multidirectional vibrations.
- Protection: Because FS65 has IP68 rating, ensure installations respect environmental sealing, protect cable runs and connection points. For FS62, ensuring cable protection against mechanical damage, moisture ingress, etc.

- Interrogation system: Optical interrogator HBM's QuantumX optical modules capable of reading FBG sensors at required wavelengths and sampling rates. Calibration needed to establish baseline (zero strain / reference temperature).
- Long-distance deployments: Because of compatibility with telecom fibre, plan for cable lengths, losses, and connectors; ensure overall signal budget (fibre attenuation, connector/coupler losses) is respected.
- Data logging: Sampling frequency must cover the 0-50 Hz range for accelerometers; for strain sensors, sampling can be lower but continuous. Storage and power for interrogator, possibly using battery or mains with safe routing.

3.3. Critical tasks and milestones

3.3.1. Critical Tasks

The implementation of the FOS monitoring campaign requires careful coordination of preparatory, technical, and validation activities. The following critical tasks and milestones have been identified:

Sensor preparation:

Critical Task 1	**Probability**	**Impact**
Verification of QuantumX MXFS interrogator functionality.	Low	High
Calibration of FS62 (strain) and FS65 (vibration) sensors to establish baseline reference values (zero strain, reference temperature).	Low	High
Contingency		
The use of well-know commercial products reduce this risk as if any problem arises, technical service from manufacturer is ensured.		

Site preparation:

Critical Task 2	**Probability**	**Impact**
Surface cleaning and preparation of steel beams for bonding of FS62 sensors.	Low	High
Definition of sensor layout, orientation, and cabling routes to minimise mechanical damage and environmental exposure.	Low	High
Contingency		
An initial site visit was performed at the beginning of this task to clearly align the methodology.		

Sensor installation:

Critical Task 3	Probability	Impact
Bonding of FS62 sensors along the longitudinal axis of the beams at predefined locations.	Low	High
Protection of optical fibres and connectors with appropriate coverings against dust, humidity, and mechanical impact.	Low	High
Placement and orientation of FS65 accelerometers in monoaxial mode to capture the primary vibration direction.	Low	High
Contingency		
The team dedicated to the installation of sensors has long experience in this field.		

Testing execution:

Critical Task 4	Probability	Impact
Execution of static loading tests to record strain profiles and validate FEM models.	Med	Med
Execution of dynamic excitation tests (impact hammer or controlled vibration) to capture modal properties.	Med	Med
Continuous acquisition of temperature and vibration data to assess sensor stability and environmental effects.	High	Med
Contingency		
On site and laboratory testing is planned.		

Processing data:

Critical Task 5	Probability	Impact
Application of FFT and time-domain analyses to vibration registers.	Med	High
Comparison of experimental data with FEM predictions and genetic algorithm calibration results.	Med	High
Identification of potential anomalies or noise in the acquired datasets.	Low	Med
Contingency		
Provide a big dataset of testing to avoid not valid data acquired.		

3.3.2. Milestones

It is presented and defined the milestones for this task, serving these for a proper monitoring of the progress of this task:

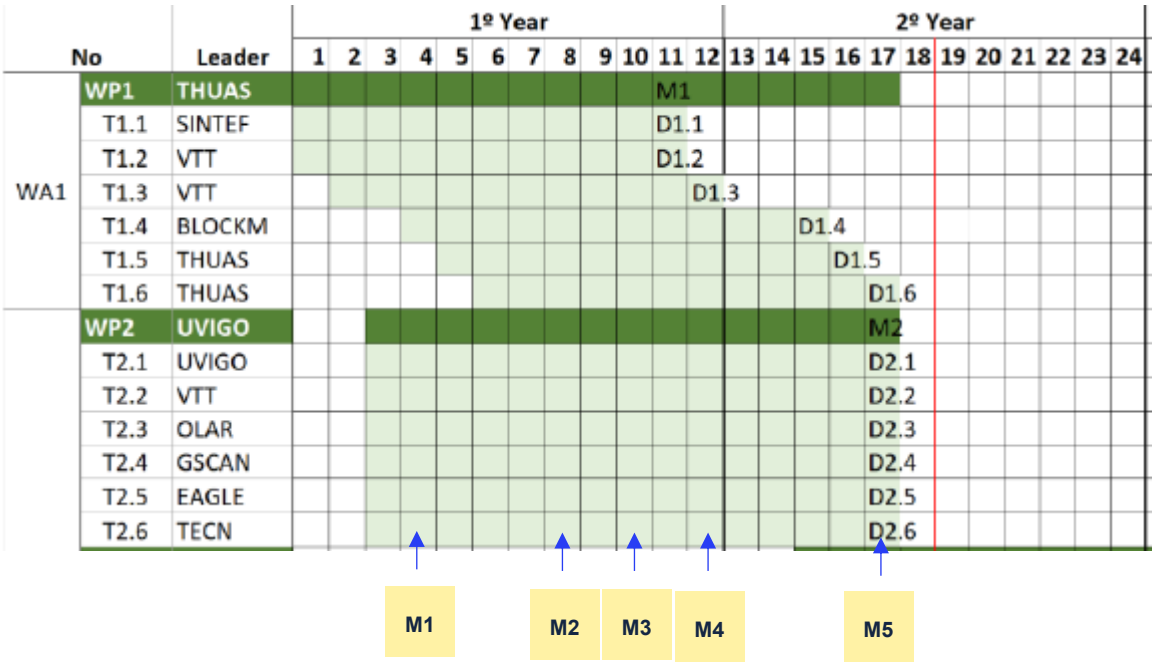

Milestones description:

- **M1** – Delivery of calibrated FOS system and interrogator (Month 4).
- **M2** – Completion of sensor installation in the Spanish pilot site (Month 8).
- **M3** – Acquisition of first static and dynamic datasets (Month 10).
- **M4** – Completion of FEM calibration with FOS data (Month 12).
- **M5** – Finalisation of Task 2.6 and delivery of D2.6 deliverable (Month 17).

4. Development

4.1. Identification of target structures

The selected element is an I-profile steel beam formerly used to support an overhead bridge crane (Figure 4). The beam is 4 meters long, with a nominal cross-section of 120 × 120 mm and a web/flange thickness of 8 mm. It was originally installed as a simply supported member; however, the as-built conditions show a partial cantilever effect at one end of approximately 20 cm, which has been accounted for in the FEM modelling. This beam is representative of heavy steel components often found in industrial facilities and targeted for reuse in new structural configurations.

Figure 4. Steel beam chosen for this research

The choice of this element was motivated by several practical and methodological considerations. First, its dimensions and length make it relatively easy to handle, transport, and reallocate in future applications, which directly aligns with the reuse strategies foreseen in Task 12.1. Second, the moderate cross-section size means that static testing can be conducted without requiring heavy equipment to apply excessively large loads, thereby simplifying the experimental setup. Third, the availability of several similar beams of the same type offers a valuable opportunity to test transfer learning methodologies in subsequent phases of the project, since comparable datasets can be generated across nominally identical elements.

Figure 5. Overview of the area, it can be noted the existence of similar steel beams

Finally, a preliminary visual inspection revealed no apparent damage or deterioration on the selected beam, confirming its suitability as a representative specimen for both experimental monitoring and FEM-based analysis.

Figure 6. Other steel beams candidate as target structures, discarded per the reason explained above.

4.2. Definition of a Risk-based assessment framework.

To ensure the robustness and reliability of the proposed FOS-based structural health monitoring system, a risk-based assessment framework was developed. This framework identifies potential risks across technical, operational, environmental, and procedural domains, assigning likelihood and impact scores to evaluate their severity. For each risk, mitigation measures were defined to reduce probability or impact, and residual risk levels were assessed after mitigation. The framework not only covers typical challenges such as fibre handling, bonding quality, and environmental degradation, but also project-specific aspects such as the dependency on T10.1 field testing for FEM calibration and the use of AI algorithms for damage detection. The resulting risk matrix provides a structured basis for monitoring implementation, quality assurance, and replication in other SUM4Re pilot sites.

Table 4. Risk-based assessment

ID	Risk Description	Category	Likelihood (L)	Impact (I)	Risk Level (L×I)	Mitigation Measures
R1	Fiber breakage during embedment	Technical	High (3)	High (3)	9 – Critical	Use protective sheaths/conduits; careful handling; personnel training
R2	Poor bonding of fibre to structure	Technical	Medium (2)	High (3)	6 – Major	Surface preparation; use proven adhesives; QA during installation

R3	Signal noise or loss during acquisition	Operational	Medium (2)	Medium (2)	4 – Moderate	High-quality connectors and splices; noise filtering algorithms
R4	Cross-sensitivity to temperature effects	Technical	Medium (2)	Medium (2)	4 – Moderate	Reference FOS sensors for temperature; software-based compensation
R5	Data Acquisition System (DAS) malfunction	Operational	Low (1)	High (3)	3 – Moderate	Redundant DAS channels; UPS backup; periodic testing
R6	Environmental degradation (water ingress, dust)	Environmental	Medium (2)	High (3)	6 – Major	IP-rated enclosures; sealants; protective casings
R7	Installation errors (human factor)	Procedural	High (3)	Medium (2)	6 – Major	SOPs; supervision; installer training; checklists
R8	Lack of access for maintenance	Operational	Medium (2)	Medium (2)	4 – Moderate	Design for accessibility; remote diagnostics
R9	Insufficient FEM calibration due to poor test data quality	Technical/Procedural	Medium (2)	High (3)	6 – Major	Integration with T10.1 on-site testing; redundancy in test campaigns; robust QA of experimental data
R10	AI-based damage identification misclassifications	Methodological	Medium (2)	High (3)	6 – Major	Hybrid models combining physics and AI; transfer learning; anomaly detection validation

4.3. Creation of predicted responses based on pool of local models

A preliminary FEM (Finite Element Method) analysis has been conducted on the two selected beams (Figure 7). The objective was to simulate expected structural responses under the proposed test loads, identify stress and strain patterns at sensor locations and support sensor layout decisions and boundary condition definitions. The model after is calibrated using nominal material properties and provides a baseline for expected sensor readings during the physical tests.

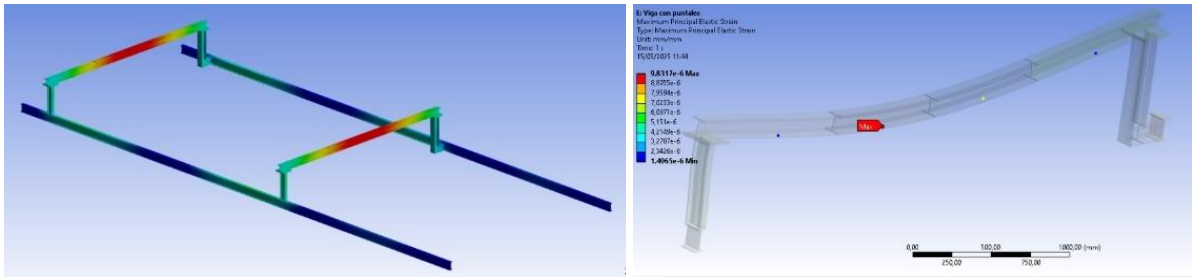

Figure 7. FEM analysis of the steel beams

The finite element model (FEM) was developed to simulate the structural response of the reused steel beam under both static and dynamic conditions. The model was used as the core of an inverse calibration framework in which selected material and boundary condition parameters were iteratively adjusted to minimize the discrepancy between numerical predictions and experimental results.

4.3.1. Modelling assumptions and geometry

A 3D linear-elastic model was implemented using commercial FEM software (ANSYS) (Figure 8). The geometry of the beam was defined as an I-profile with a total length of 4 meters, a web height and flange width of 120 mm, and a uniform thickness of 8 mm. Solid elements were used to represent the beam geometry with sufficient fidelity while maintaining computational efficiency for multiple iterations during the calibration process.

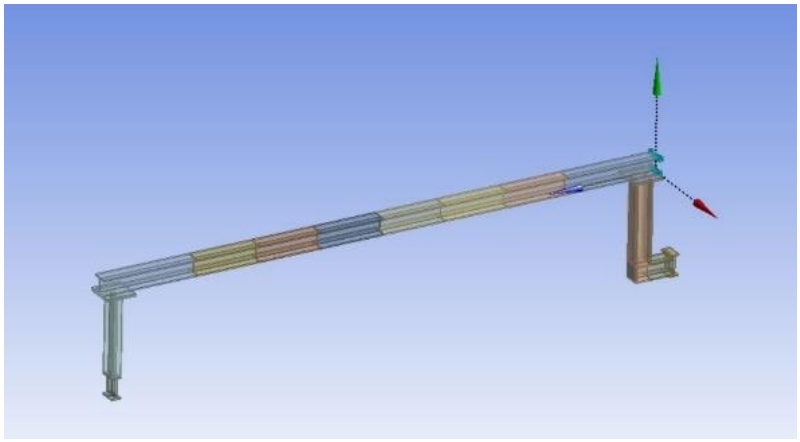

Figure 8. Steel beam modelling

The steel was modelled as linearly elastic, with Young's modulus (E) treated as a calibration parameter. The initial value of E was set to the standard structural steel modulus of 210 GPa, per Eurocode recommendations. Poisson's ratio was fixed at 0.3, and density was taken as 7850 kg/m³. No material nonlinearity or plastic deformation was included in this phase of modelling, as the experimental tests were within the elastic regime.

4.3.2. Boundary conditions and loading

The beam was simply supported in the initial model configuration. However, due to field variability and the beam's partial cantilever condition at one end (approximately 20 cm), the support stiffness was recognized as a potential source of uncertainty. During the experiment, auxiliary columns were placed directly under the beam supports to isolate its response and enforce conditions as close as possible to ideal simple supports.

These boundary conditions were subject to calibration during the FEM updating process, as small deviations in rotational restraint or vertical flexibility could influence both static deformations and natural frequencies. As per future research activities, support conditions can be represented using elastic springs with tunable stiffness to approximate realistic behaviour where required. Nevertheless, in this case, the focus of the calibration parameter has been the young modulus, and modifications applied at boundary conditions have been focused on variations of restrictions / releases of rotational degrees or longitudinal axis at the supports.

In the static simulations, point loads were applied at positions matching the test setup to replicate the three-point bending scenarios. In the dynamic analysis, a modal extraction was performed to compute the natural frequencies and corresponding mode shapes.

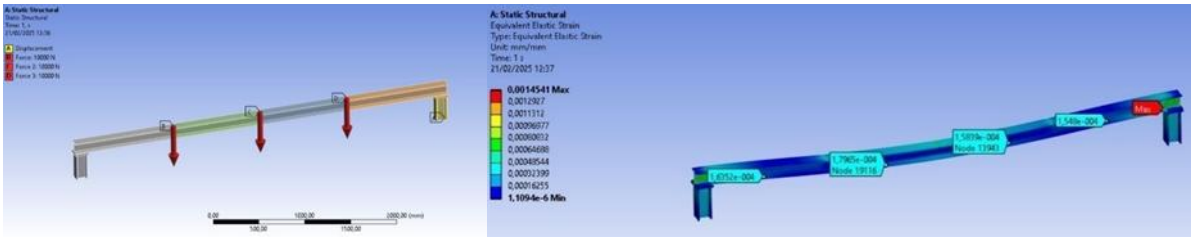

Figure 9. Static modelling. The output is parametrized as the elastic strain at the axis and exact location of the fibre optic strain sensors installed on the physical steel beam, which will support the inverse modelling calibration.

4.3.3. Preliminary static modelling

The preliminary Finite Element Method (FEM) analysis served multiple critical purposes: informing the optimal placement of Fibre Optic Sensors (FOS), defining the expected range of structural behaviour, and establishing a baseline dataset for the subsequent inverse-modelling and calibration phase.

After an initial site visit to measure the details required for modelling the target beam, a preliminary model was performed to design the static testing in terms of maximum load to be applied (to not to overpass elastic limit of the beam, supposed to be under 275 MPa, a typical value of this kind of structural elements) and also the expected range of strain.

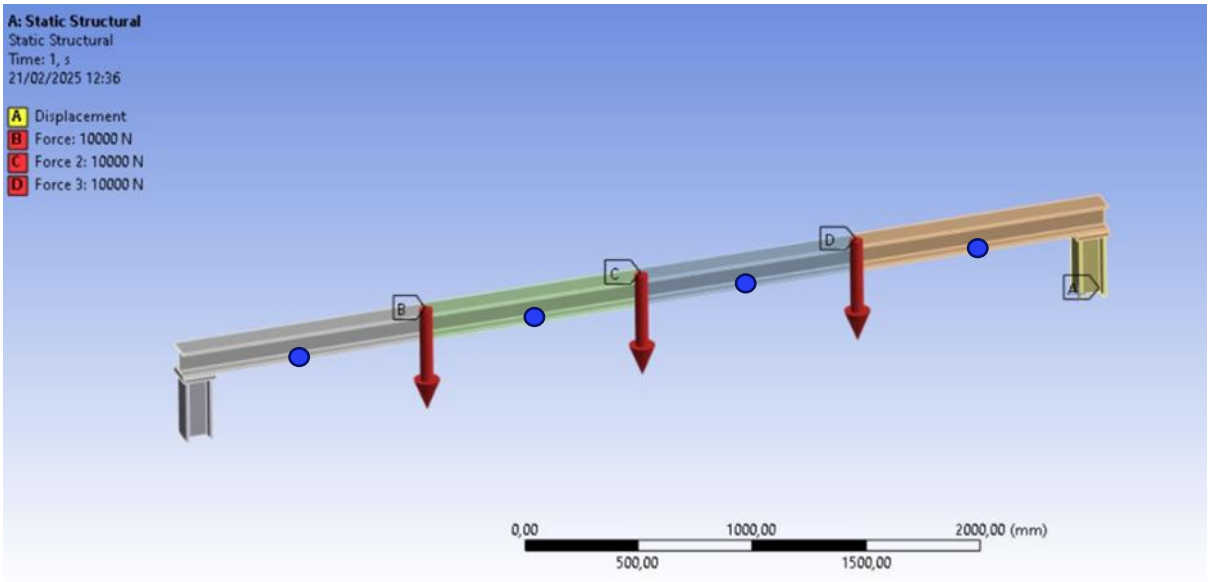

Figure 10. Static modelling testing applying 10KN at the three points load with equidistant distribution along the length of the beam (4.27m). Blue circles represent the installation points of the FOS sensors.

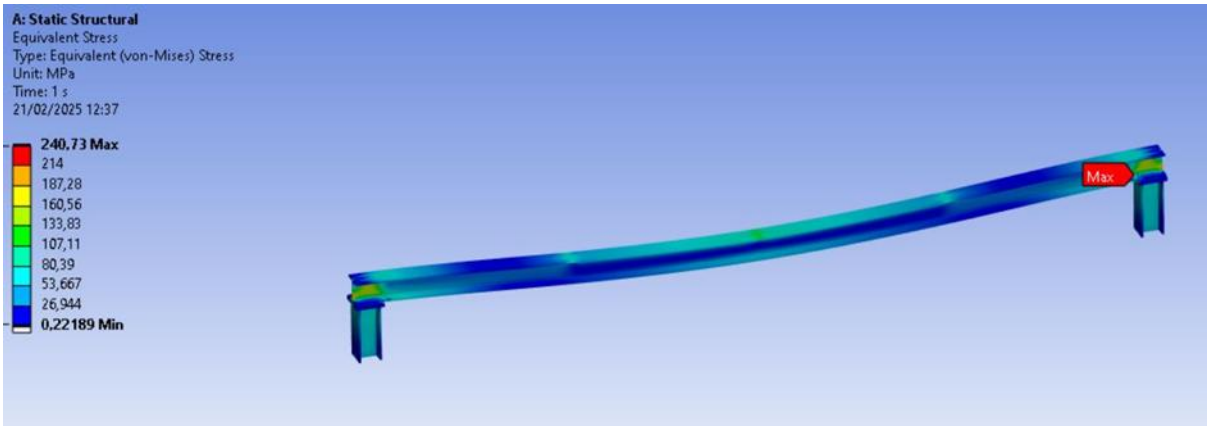

Figure 11. Maximum stress expected

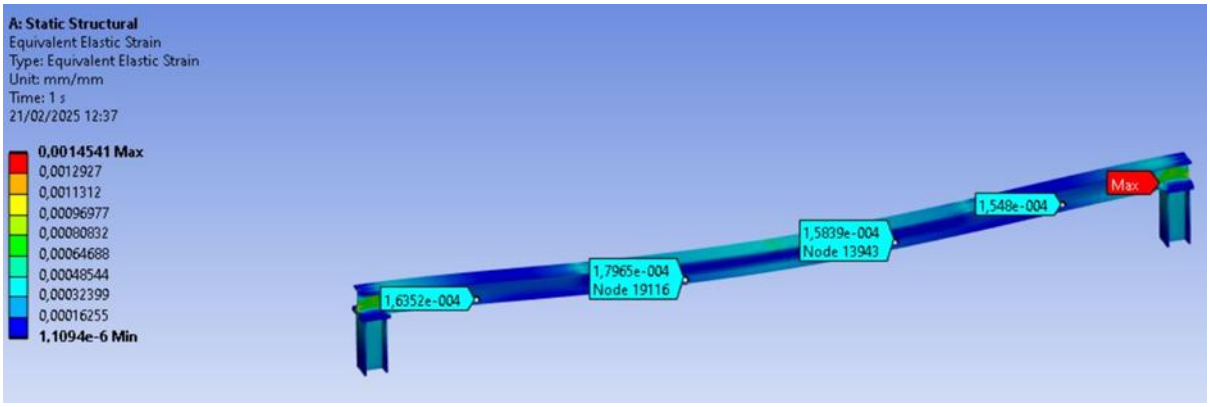

Figure 12. Expected maximum strain at the points where the FOS sensors are decided to be installed (equidistant to load application point according to Figure 10).

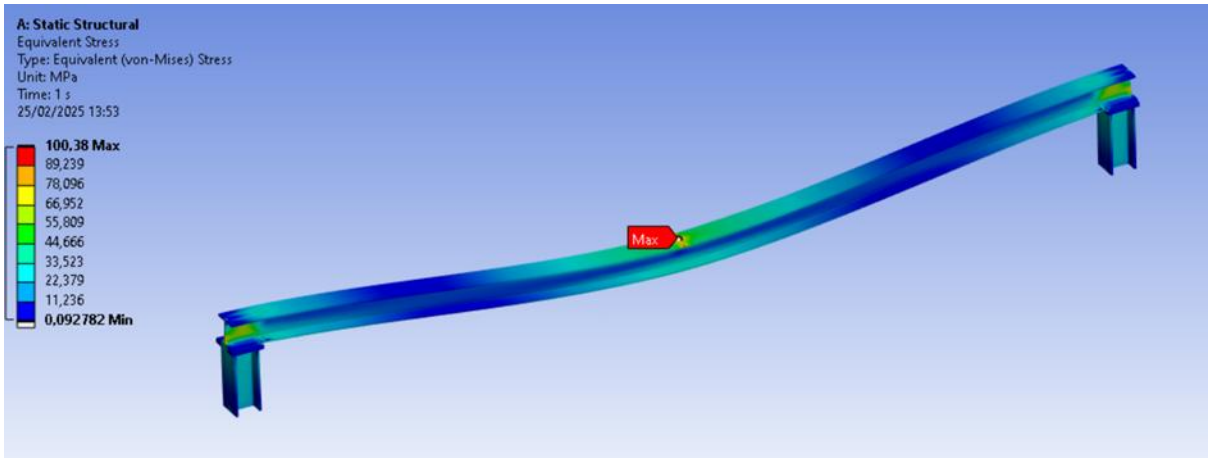

Figure 13. Applied load at only the middle point (10KN)

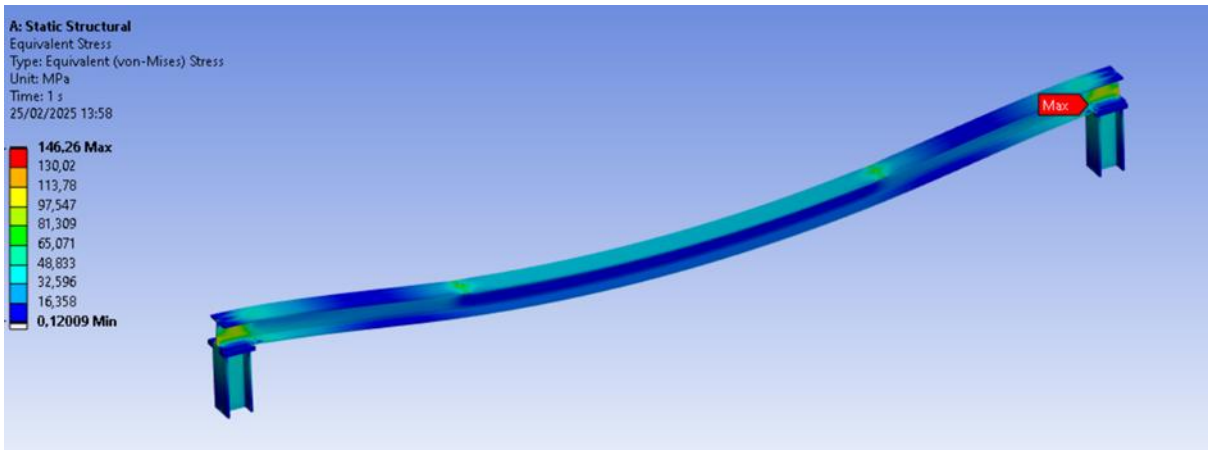

Figure 14. Applied load at L/4 and 3L/4 stress

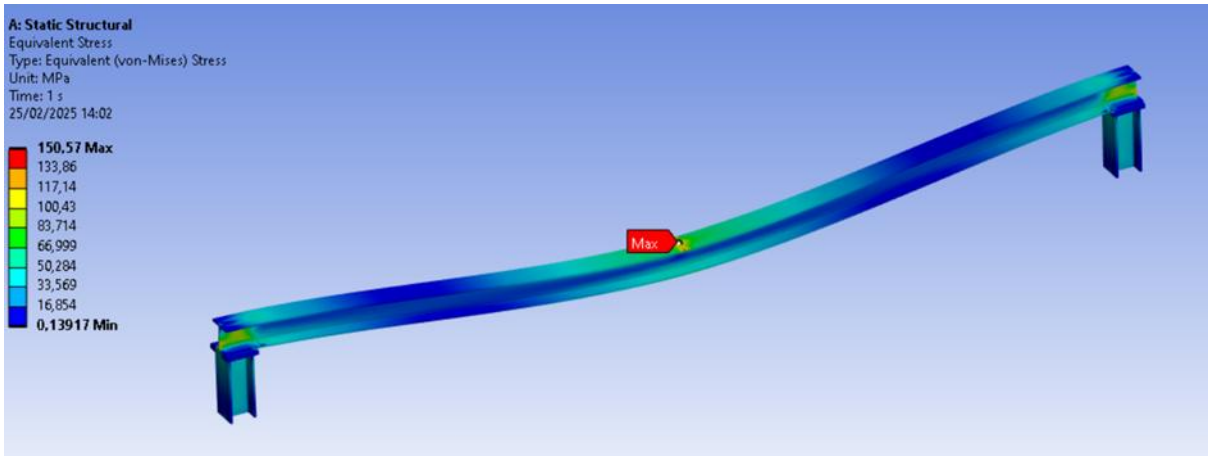

Figure 15. Applied load of 15KN at the middle point

This pool of local models resulted in a comprehensive library of possible structural behaviours. This library was essential for:

- Sensor layout optimization: Confirming that the chosen sensor locations were sensitive to the parameters intended for calibration (as per Figure 11).

- Defining the calibration space: Providing the "predicted responses" against which the real experimental data from the FOS would be compared during the algorithm-based calibration process described in Section 4.4.
- Sensitivity analysis: Identifying which parameters (e.g., E vs. boundary stiffness) had the most significant influence on the structural response, thereby guiding the focus of the calibration effort.

The creation of the preliminary models ensured that the subsequent experimental and calibration phases were conducted efficiently and with a clear understanding of the possible structural states.

4.3.4. Modal analysis and mode selection

A preliminary modal analysis was carried out for the full frequency range of interest. The results yielded a large number of mode shapes, including torsional and higher-order local modes. To ensure a meaningful comparison with experimental data and reduce model complexity, a mode participation analysis was conducted.

Only the modes with the highest modal participation ratios in the vertical direction (Z-axis) and the horizontal direction (X axis) were retained for calibration. These typically correspond to the first and second flexural modes, which dominate the dynamic response of simply supported beams under vertical and horizontal excitation. Modes with negligible dynamic contribution or those predominantly involving torsion or local flange vibration were discarded.

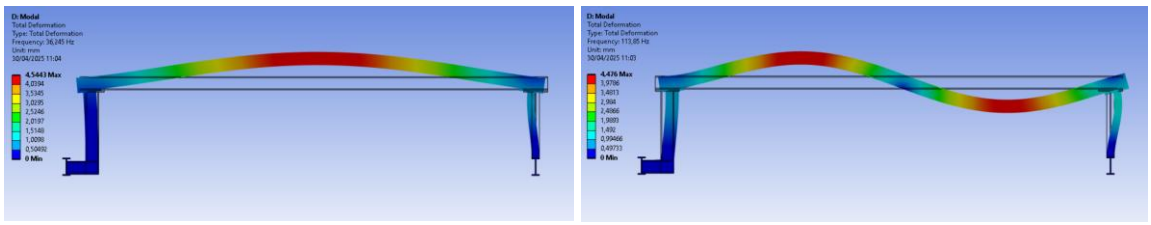

MODE	FREQUENCY	PERIOD	PARTIC.FACTOR	RATIO	EFFECTIVE MASS	MASS FRACTION	TO TOTAL MASS
1	14.3927	0.69480E-01	0.30257	1.000000	0.915484E-01	0.678921	0.564811
2	36.2453	0.27590E-01	-0.19759E-04	0.000065	0.390433E-09	0.678921	0.240879E-08
3	38.0776	0.26262E-01	0.88768E-01	0.293381	0.787981E-02	0.737357	0.486147E-01
4	42.4020	0.23584E-01	-0.35508E-01	0.117356	0.126085E-02	0.746708	0.777886E-02
5	54.5340	0.18337E-01	-0.14324E-06	0.000000	0.205168E-13	0.746708	0.126579E-12
6	63.5299	0.15741E-01	0.14786	0.488684	0.218629E-01	0.908843	0.134884
7	92.6084	0.10798E-01	0.45788E-01	0.151329	0.209651E-02	0.924390	0.129345E-01
8	104.263	0.95912E-02	0.82014E-01	0.271060	0.672637E-02	0.974273	0.414986E-01
9	113.846	0.87838E-02	-0.10755E-04	0.000036	0.115673E-09	0.974273	0.713648E-09
10	150.041	0.66649E-02	0.58899E-01	0.194664	0.346914E-02	1.00000	0.214030E-01

Figure 16. Preliminary modal analysis performed for E=210 GPa. Results obtained for first and second modal shapes (vertical axis) and extracted table of modal participation factor table.

In addition to the vertical modes, it has been identified that the horizontal mode shapes are also relevant and scope of calibration:

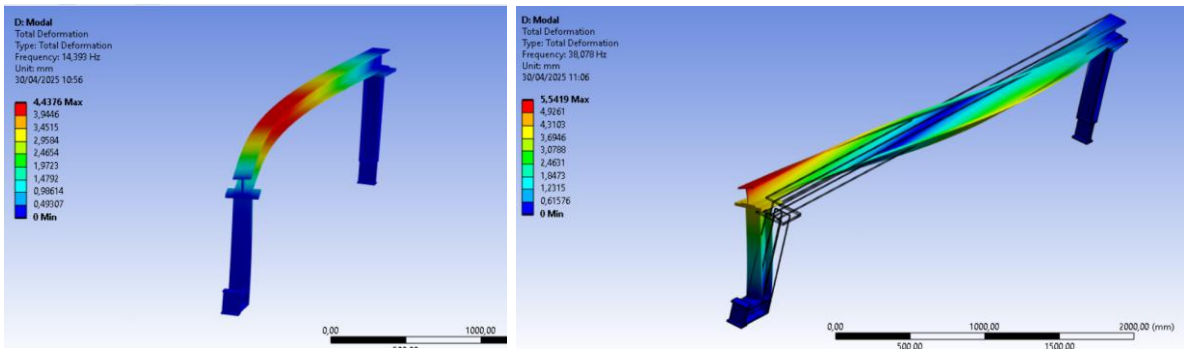

***** PARTICIPATION FACTOR CALCULATION *****							
MODE	FREQUENCY	PERIOD	PARTIC.FACTOR	CUMULATIVE RATIO	X EFFECTIVE MASS	DIRECTION EFF.MASS	
FRACTION		TO		TOTAL		MASS	
1	14.3927	0.69480E-01	0.30257	1.000000	0.915484E-01	0.678921	0.564811
2	36.2453	0.27590E-01	-0.19759E-04	0.000065	0.390433E-09	0.678921	0.240879E-08
3	38.0776	0.26262E-01	0.88768E-01	0.293381	0.787981E-02	0.737357	0.486147E-01
4	42.4020	0.23584E-01	-0.35508E-01	0.117356	0.126085E-02	0.746708	0.777886E-02
5	54.5340	0.18337E-01	-0.14324E-06	0.000000	0.205168E-13	0.746708	0.126579E-12
6	63.5299	0.15741E-01	0.14786	0.488684	0.218629E-01	0.908843	0.134884
7	92.6084	0.10798E-01	0.45788E-01	0.151329	0.209651E-02	0.924390	0.129345E-01
8	104.263	0.95912E-02	0.82014E-01	0.271060	0.672637E-02	0.974273	0.414986E-01
9	113.846	0.87838E-02	-0.10755E-04	0.000036	0.115673E-09	0.974273	0.713648E-09
10	150.041	0.66649E-02	0.58899E-01	0.194664	0.346914E-02	1.00000	0.214030E-01

Figure 17. Preliminary modal analysis performed for E=210 GPa. Results obtained for first and second modal shapes (horizontal axis) and extracted table of modal participation factor table.

The initial modal analysis was conducted under the idealized assumption of simply supported boundary conditions, which predicted distinct vertical and horizontal bending modes characteristic of such constraints. However, recognizing that the actual structural behaviour in the field would be influenced by the complex connectivity and continuity of the full crane beam system, a more sophisticated model was developed. This subsequent analysis accounted for the non-ideal, non-simply supported conditions by modelling the complete structural assembly, including connections to supporting columns and adjacent members.

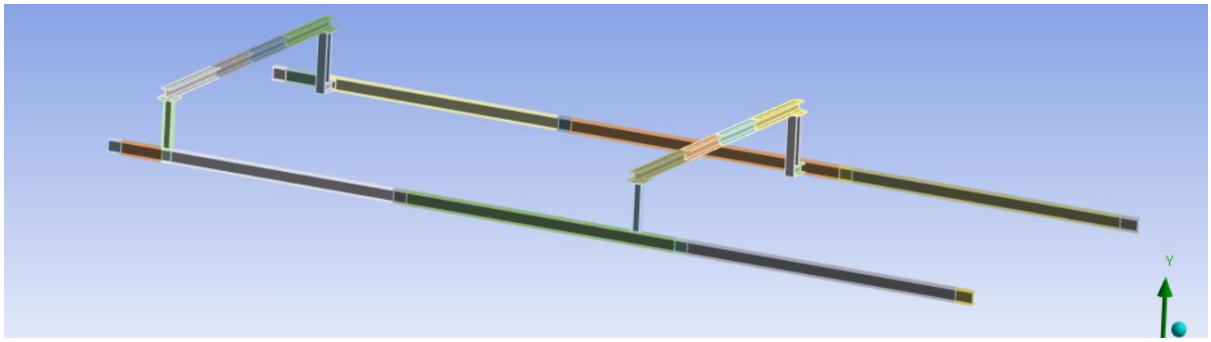

Figure 18. Modelling of the full beam crane system

Obtained results show a very similar values (as local mode shapes) than the simply supported case.

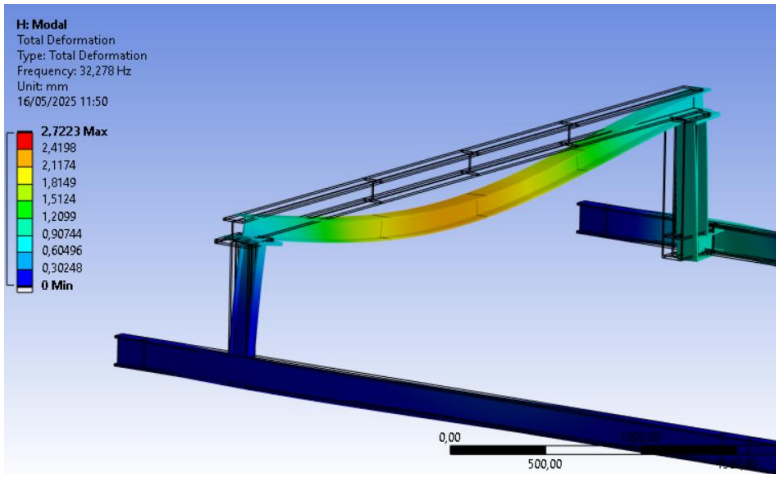

Figure 19. Obtained first vertical bending mode

In light of the modal analysis results, which identified the first and second flexural modes as dominant in the structural response, the monitoring plan for the dynamic characterization was strategically defined. The objective is to capture sufficient modal information to effectively calibrate the numerical model. To this end, accelerometers will be deployed at two critical locations: one at mid-span (L/2) and a second at the quarter-span (L/4). This configuration is optimal as the L/2 position exhibits maximum displacement for the fundamental mode, while the L/4 point provides a non-zero measurement for the second mode and allows for reliable distinction between symmetric and anti-symmetric mode shapes. This two-sensor setup provides the necessary spatial resolution to accurately identify the key modal frequencies and validate the corresponding mode shapes obtained from the finite element model

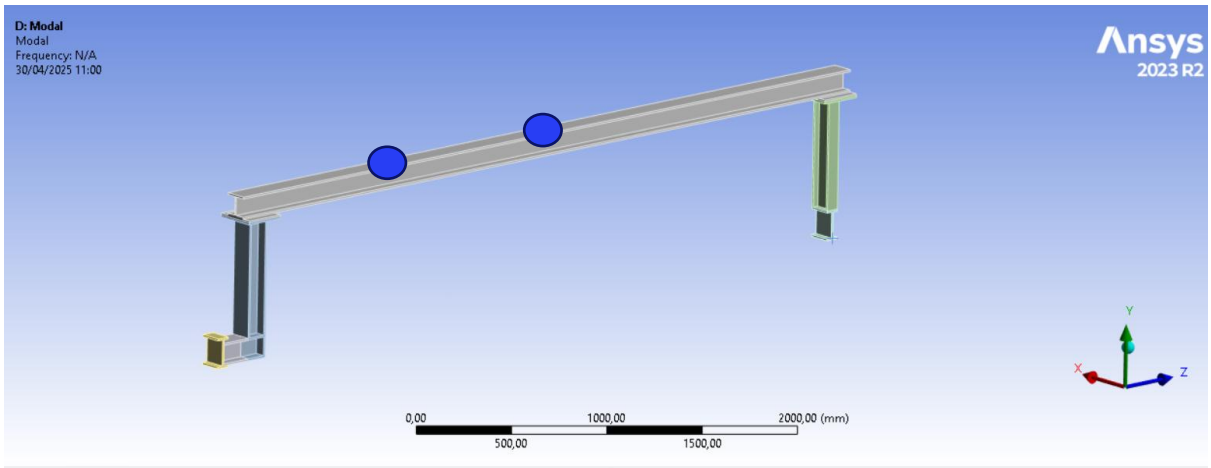

Figure 20. Proposed installation location for accelerometers at L/2 and L/4

Figure 21. Detail of installed accelerometers (on top of the beam)

4.4. Installation and inverse-modelling for calibration of the system

An inverse calibration procedure has been defined to refine the FEM model using real test data (more information can be found in deliverable D10.1). The approach includes simulated response comparisons to physical test results for optimization of material parameters. This process is essential to ensure a high-fidelity numerical model aligned with the real behaviour of the tested beams. Once the inverse calibration is complete and the FEM model validated, the next step will involve the analysis and implementation of a damage identification algorithm.

The primary objective of the calibration process was to determine the Young's modulus (E) that best replicates the structural behaviour measured during experimental tests of the use case proposed in WA6. To this end, a direct error-minimization strategy was employed, comparing simulated responses from FEM with experimental data acquired through FOS during both static loading and dynamic testing.

The calibrated FEM sets the foundation for data-driven damage detection. An artificial intelligence (AI) module based on autoencoder neural networks has been developed to detect anomalous structural responses. The model will initially be trained using synthetic simulations of undamaged (healthy) states. Reconstruction errors from the autoencoder will be analysed to flag potential anomalies indicative of damage.

4.4.1. Experimental results

The static characterization involved a three-point bending configuration, a standard method for determining flexural stiffness in beam elements. Loads were applied using fastening straps connected to ground-anchored steel base plates via steel ropes, simulating point loads. The anchorage system was designed to be flexible and non-invasive, minimizing interference with the test element. The ropes were routed over the beam to apply the load at designated locations, and load cells were installed at each loading point to continuously measure the applied force.

Figure 22. Static test installed on site and installed steel plates on the ground

The test protocol consisted of distinct load scenarios, varying the magnitude of the applied forces to generate a comprehensive strain profile across the beam. These scenarios were used to capture the global and local stiffness characteristics of the beam under typical reuse-relevant loading configurations. Below it is presented an example of one of the performed static tests, more information can be found in deliverable D10.1.

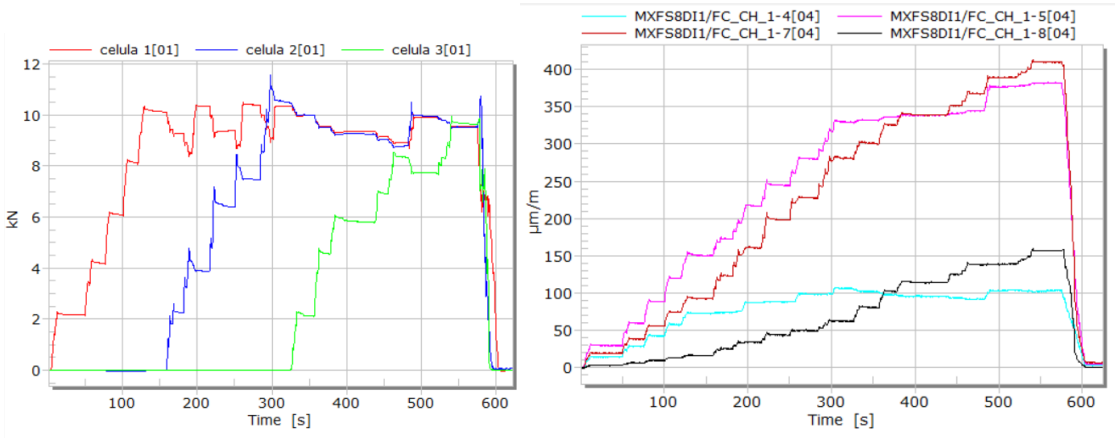

Figure 23. Examples of loading – strain measured static testing

For dynamic testing, the beam was instrumented with two fibre optic accelerometers positioned at midspan (1/2L) and quarter-span (1/4L), allowing for the capture of relevant mode shapes and natural frequencies. A manual impact hammer was used to excite the beam, simulating an impulsive load, and the resulting free vibrations were recorded. Data acquisition was synchronized across all sensors to ensure temporal consistency between excitation and response [12].

The following figures summarize some of the outputs of the experimental campaign and their comparison with FEM predictions for both dynamic and static testing.

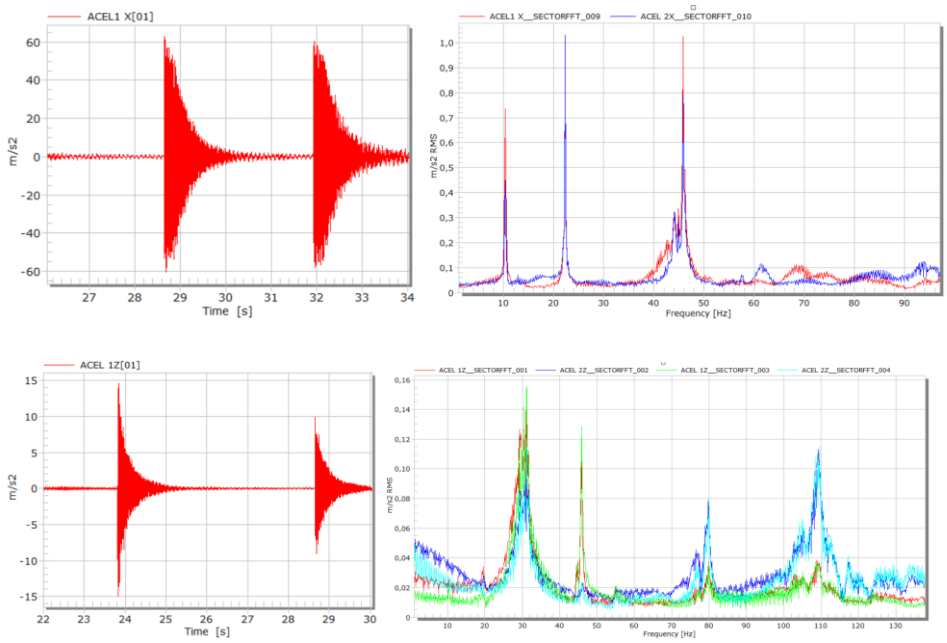

Figure 24. Left graphs: Horizontal and vertical acceleration registers over time. Right: FFT analysis content extracted from free vibration register.

The experimental modal analysis conducted via FFT processing of acceleration data identified the first two vertical flexural modes of the beam as the most significant for structural calibration [13]. The measured natural frequencies for these modes were: First flexural mode: 10.4 Hz; second flexural mode: 31.05 Hz. These values serve as reference targets for the dynamic calibration process. The finite element model is adjusted to replicate these frequencies by tuning both the Young's modulus (E) and the effective support conditions, ensuring accurate representation of global stiffness and boundary flexibility. The emphasis on flexural modes aligns with the expected deformation behaviour under vertical loading and impact excitation.

In parallel, the static test results—specifically the strain responses under the distinct loading cases—are used to refine the Young's modulus based on a best-fit strategy. The integration of both static and dynamic data within a unified FEM calibration framework improves model robustness and enables a more reliable estimation of mechanical properties and support behaviour, which are critical for assessing the beam's reuse potential.

The FEM calibration process allowed for a refined estimation of mechanical parameters, particularly the Young's modulus, which was updated based on experimental evidence. This enhanced model now more accurately reflects the structural behaviour of the monitored element and can be used to assess residual load-bearing capacity and evaluate safety margins.

4.4.2. Integrated Static–Dynamic FEM calibration

The FEM was iteratively solved for 30 values of Young's modulus across a realistic range, from 100 GPa to 210 GPa. For each E value, both static strain distributions and natural frequencies were computed and compared with experimental data using error metrics. Support conditions

were also fine-tuned based on discrepancies between expected and measured modal behaviour, as previously explained in section 4.3.2.

This hybrid calibration strategy, based on both static and dynamic responses, allowed the final model to represent the actual mechanical behaviour of the beam with high fidelity. The aim of the calibration process is to determine the Young's modulus (E) that best reproduces the structural behaviour observed during both static and dynamic tests. To achieve that, we employ a direct error-minimization approach based on experimental and numerical comparisons.

Two sources of experimental data were used: strain measurements from different static loading scenarios, and the first two natural frequencies from dynamic characterization. For each of the candidate values of E, numerical simulations were conducted to generate corresponding synthetic responses. These were compared with the experimental measurements using two standardized error metrics: root mean squared error (RMSE) and mean absolute error (MAE).

The calibration seeks to minimize the discrepancy between measured and simulated data, independently for static and dynamic cases. Subsequently, both sources are integrated into a unified framework to identify an optimal E value that balances accuracy across datasets.

Table of Outline A2: Design Points of Design of Experiments

	A	B	C	D	E	F	G	H	I	J	K
1	Name	P58 - Force Y Component (N)	P59 - Force 2 Y Component (N)	P60 - Force 3 Y Component (N)	P67 - Young's Modulus (Pa)	P61 - Total Deformation Reported Frequency (Hz)	P62 - Normal Elastic Strain Maximum (mm mm^-1)	P63 - No... El... St... 2 M... (mm mm^-1)	P64 - Normal Elastic Strain 3 Maximum (mm mm^-1)	P65 - Normal Elastic Strain 4 Maxim... (mm mm^-1)	P66 - Total Deform... 2 Reported Frequency (Hz)
2	1	-9156	-6108	-11676	1,659E+11						
3	2	-5916	-10068	-8748	1,965E+11						
4	3	-11844	-4620	-4236	1,625E+11						
5	4	-7596	-5988	-11916	1,209E+11						
6	5	-8964	-10668	-1476	1,141E+11						
7	6	-444	-2100	-3996	1,399E+11						
8	7	-11052	-1548	-5100	1,679E+11						
9	8	-1116	-7788	-10932	1,339E+11						
10	9	-10092	-540	-7668	1,727E+11						
11	10	-10188	-516	-5244	1,481E+11						
12	11	-9276	-3876	-3924	1,055E+11						
13	12	-11412	-3636	-4068	1,847E+11						
14	13	-10068	-6036	-11028	1,863E+11						
15	14	-11796	-4044	-6948	1,691E+11						
16	15	-8508	-6732	-5556	1,191E+11						
17	16	-3468	-5676	-2268	1,755E+11						
18	17	-2508	-1116	-10476	1,613E+11						
19	18	-6756	-1476	-5628	1,061E+11						
20	19	-2220	-5844	-9588	1,953E+11						
21	20	-11580	-9588	-5940	1,183E+11						
22	21	-9324	-5940	-3636	1,643E+11						
23	22	-204	-7020	-7764	1,261E+11						
24	23	-828	-6252	-2148	1,127E+11						
25	24	-7212	-324	-7212	1,503E+11						
26	25	-5148	-11676	-4044	1,173E+11						
27	26	-6348	-2460	-10740	1,081E+11						
28	27	-3324	-11628	-2556	1,321E+11						

Figure 25. Synthetic scenarios launched in ANSYS FEM

4.4.3. Error minimization

The static responses consist of strain values at selected sensor locations under 15 loading scenarios. The dynamic responses include the first two natural frequencies of the beam. For each of the 30 candidate values of Young's modulus E, finite element simulations are performed to

generate synthetic static and dynamic responses. These are then compared with the corresponding experimental results.

To evaluate the agreement between simulation and experiment, it is computed two standard error metrics: the root mean squared error (RMSE) and the mean absolute error (MAE). Both static and dynamic datasets are standardized prior to error computation to ensure comparability of values. The full distribution of static errors is retained to capture variability across loading conditions.

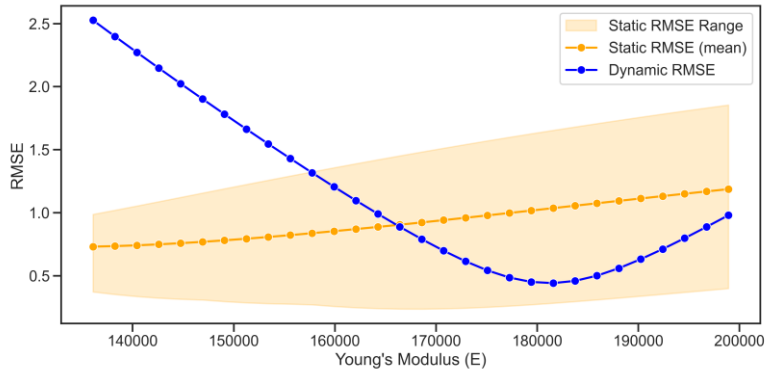

Figure 26. Evolution of RMSE as a function of E for both static and dynamic calibrations

The figure shows that the static RMSE increases as E increases, with the best fit around 136 GPa. In contrast, the dynamic RMSE reaches its minimum near 181 GPa and increases steadily with higher stiffness values. The shaded band in the static curve represents the range of RMSE values across all load conditions, reflecting the variability in fit quality for different scenarios. These results indicate that no single value of E simultaneously minimizes both error curves. A trade-off must be established to determine the optimal value for calibration.

Table of Outline A2: Design Points of Design of Experiments

	A	B	C	D	E	F	G	H	I	J	K
1	Name	P58 - Force Y Component (N)	P59 - Force 2 Y Component (N)	P60 - Force 3 Y Component (N)	P67 - Young's Modulus (Pa)	P61 - Total Deformation Reported Frequency (Hz)	P62 - Normal Elastic Strain Maximum (mm mm^ -1)	P63 - No... El... St... 2 M... (mm mm^ -1)	P64 - Normal Elastic Strain 3 Maximum (mm mm^ -1)	P65 - Normal Elastic Strain 4 Maxim... (mm mm ^-1)	P66 - Total Deform... 2 Reported Frequency (Hz)
2	1	-9156	-6108	-11676	1,659E+11						
3	2	-5916	-10068	-8748	1,965E+11						
4	3	-11844	-4620	-4236	1,625E+11						
5	4	-7596	-5988	-11916	1,209E+11						
6	5	-8964	-10668	-1476	1,141E+11						
7	6	-444	-2100	-3996	1,399E+11						
8	7	-11052	-1548	-5100	1,679E+11						
9	8	-1116	-7788	-10932	1,339E+11						
10	9	-10092	-540	-7668	1,727E+11						
11	10	-10188	-516	-5244	1,481E+11						
12	11	-9276	-3876	-3924	1,055E+11						
13	12	-11412	-3636	-4068	1,847E+11						
14	13	-10068	-6036	-11028	1,863E+11						
15	14	-11796	-4044	-6948	1,691E+11						
16	15	-8508	-6732	-5556	1,191E+11						
17	16	-3468	-5676	-2268	1,755E+11						
18	17	-2508	-1116	-10476	1,613E+11						
19	18	-6756	-1476	-5628	1,061E+11						
20	19	-2220	-5844	-9588	1,953E+11						
21	20	-11580	-9588	-5940	1,183E+11						
22	21	-9324	-5940	-3636	1,643E+11						
23	22	-204	-7020	-7764	1,261E+11						
24	23	-828	-6252	-2148	1,127E+11						
25	24	-7212	-324	-7212	1,503E+11						
26	25	-5148	-11676	-4044	1,173E+11						
27	26	-6348	-2460	-10740	1,081E+11						
28	27	-3324	-11628	-2556	1,321E+11						

Figure 27. Synthetic scenarios launched in ANSYS with different loading scenarios and different Young Modulus, with output of the two target natural frequencies and the strain measurement at the sensor locations.

The initial comparison between the static and dynamic testing results revealed a significant discrepancy in the estimated Young's modulus values. While the static loading tests suggested a considerably lower modulus, the dynamic modal analysis yielded a higher stiffness value. This divergence can be attributed to the assumptions made in the FEM modelling, particularly regarding the boundary conditions. The beam was initially modelled as perfectly simply supported; however, the as-built inspection and test results indicated that the actual support conditions did not fully correspond to this idealisation. Factors such as partial fixity at the supports, residual stresses from fabrication, and minor eccentricities in the end restraints can strongly influence the apparent stiffness observed under static loading, thereby leading to an underestimation of the material modulus.

To address this issue, alternative boundary condition scenarios were evaluated in the FEM calibration process. These included combinations of simple support with partial rotational restraint, as well as models accounting for a limited cantilever effect at one end, consistent with the observed installation. By refining the boundary conditions as per section 4.3.2, the calibration produced a much closer agreement between the static and dynamic test results. The updated RMSE analysis (Figure 28) shows that the gap between the two estimates of Young's modulus is significantly reduced, converging towards a value of approximately 155 GPa.

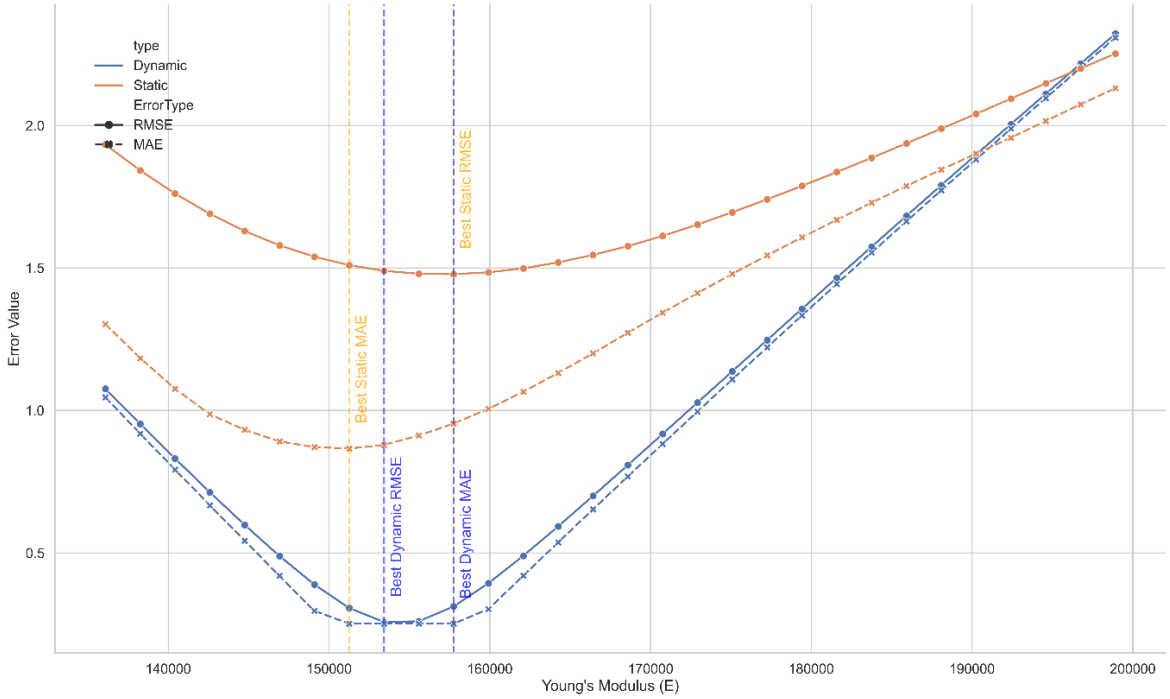

Figure 28. Final RMSE / MAE obtained for static and dynamic calibration datasets

This revised modulus is considered reasonable given the steel type and age of the structure. The industrial building from which the beam was recovered was constructed in the 1950s, a period when typical structural steels used in the Basque Country often exhibited elastic moduli in the range of 150–160 GPa. The final calibrated value is therefore consistent both with the material's historical context and with the expected performance of comparable structural steels, providing confidence in the validity of the FEM model and the monitoring approach.

4.4.4. Weighted Error Aggregation and Parameter Estimation

Since the static and dynamic error curves reach their minima at different values of E, a combined error metric is proposed to guide the selection of an optimal stiffness. The total error is computed as a weighted sum of the static and dynamic RMSE values for each tested E:

$$RMSE_{total}(E) = w_s \cdot RMSE_{static}(E) + w_d \cdot RMSE_{dynamic}(E)$$

where w_s and w_d are scalar weights that reflect the relative importance or confidence in the static and dynamic datasets. In this study, equal weights ($w_s = w_d = 0.5$) are applied to give balanced influence on both sources of information. All RMSE values are computed using standardized data to ensure consistent scaling.

The combined RMSE curve allows identification of the E value that minimizes the total error. The optimal Young's modulus is found to lie between the static-only and dynamic-only minimal, reflecting a compromise between both calibration objectives. This value represents the best

overall match between simulation and experiment when considering both types of structural response.

This approach provides a simple yet effective framework for integrating multiple experimental datasets in model calibration. It also highlights the sensitivity of the optimal parameter to the chosen error weighting, suggesting that adjustments could be made in future work based on data quality or application-specific priorities.

To obtain a singular value of the Young's modulus for calibration, an optimization strategy was followed in which both static and dynamic error metrics (RMSE and MAE) were considered simultaneously. The individual curves showed that the dynamic RMSE reached its minimum at approximately 152–154 GPa, while the dynamic MAE was slightly shifted towards higher values (~156–158 GPa). For the static case, the minima of both RMSE and MAE were also spread across the 151–158 GPa range. This dispersion indicated that choosing the minimum of a single metric (e.g. dynamic RMSE only) would necessarily degrade the fit in the other metrics, resulting in an unbalanced calibration.

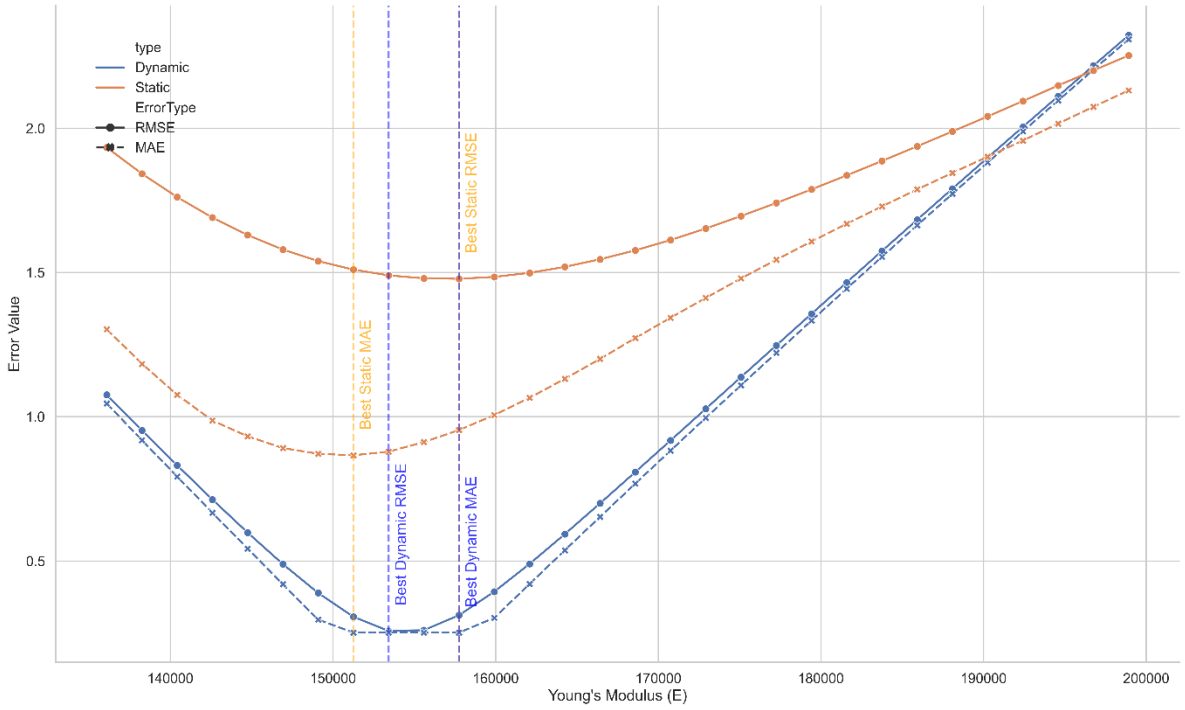

To address this, a combined objective function was defined:

$$J(E) = w_s \cdot \frac{\mathrm{RMSE}_{\mathrm{static}}(E)}{\max(\mathrm{RMSE}_{\mathrm{static}})} + w_d \cdot \frac{\mathrm{RMSE}_{\mathrm{dynamic}}(E)}{\max(\mathrm{RMSE}_{\mathrm{dynamic}})}$$

where the RMSE values were normalised to allow direct comparison, and w_s, w_d, represent weighting factors for the static and dynamic responses. In extended form, the objective function can also include the MAE terms:

$$J(E) = \alpha \cdot \tilde{\mathrm{RMSE}}_{dyn} + \beta \cdot \tilde{\mathrm{MAE}}_{dyn} + \gamma \cdot \tilde{\mathrm{RMSE}}_{stat} + \delta \cdot \tilde{\mathrm{MAE}}_{stat}, \quad \alpha + \beta + \gamma + \delta = 1$$

where the tilde indicates normalization of each metric. In this study, equal weights were assigned to static and dynamic performance, as both responses are considered equally important for model fidelity. The resulting normalized error curve (Figure 29) exhibited a clear minimum at approximately E ≈ 155 GPa, which was therefore chosen as the recommended compromise value.

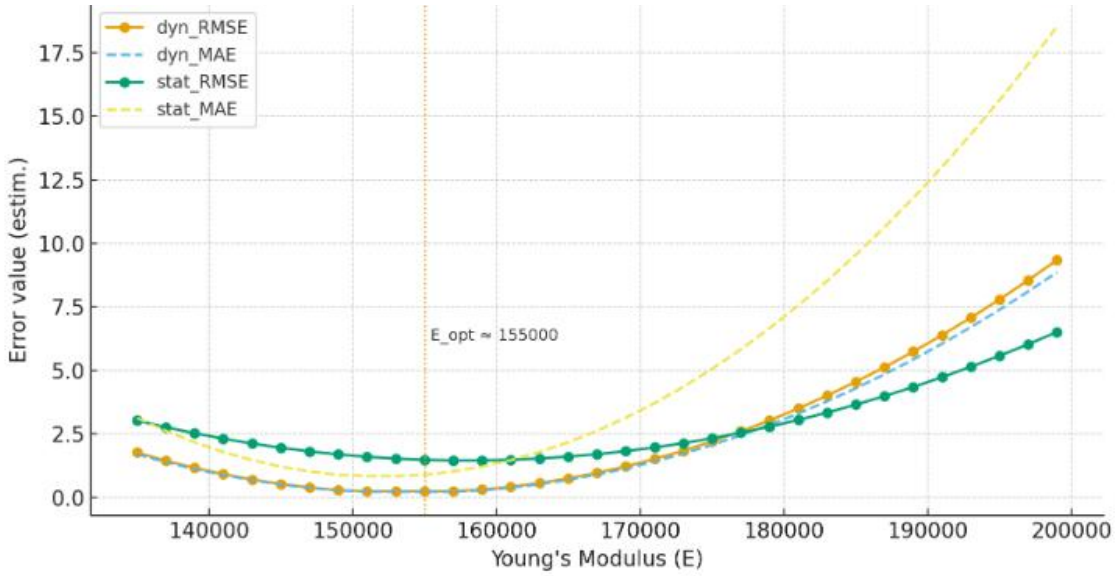

Figure 29. Normalised error RMSE - MAE

This value lies between the minima of the individual criteria, ensuring that the FEM model performs consistently well for both static and dynamic responses. It represents a balanced trade-off between accuracy in the two domains and avoids biasing the calibration towards either load-displacement curves or vibration characteristics. Importantly, the final modulus of 155 GPa is also in line with the expected range for steels used in industrial buildings constructed in the Basque Country during the 1950s, which typically exhibit elastic moduli between 150–160 GPa. This provides further confidence that the selected value is both technically justified and historically consistent with the material properties of the pilot structure.

The selection of a compromise value of E ≈ 155 GPa is also particularly relevant for the activities foreseen in Task 3.6 of WP3, where transfer learning methods will be trained and validated. The availability of a calibrated Young's modulus consistent with both static and dynamic responses ensures that the structural behaviour captured by the FEM model reflects realistic stiffness

properties of the steel beams. This reduces the bias introduced by inaccurate material assumptions and provides a reliable baseline dataset for domain adaptation. By grounding the training of transfer learning models on a well-validated modulus value, the methodology can more effectively generalise to other beams of similar typology, thereby strengthening the application of AI-driven anomaly detection and cross-structure comparisons across the SUM4Re pilots.

4.5. Damage identification applying AI-techniques to the collected structural response data.

The final step of the integrated SHM framework developed in Task 2.6 concerns damage identification [14], building on the calibrated FEM models and the structural response data collected by the fibre optic sensors. The aim is to detect early signs of degradation or damage in structural elements, thereby supporting safe reuse and extending service life within circular construction strategies.

To achieve this, the project adopts an AI-based anomaly detection approach, with a particular focus on unsupervised learning methods that do not require labelled damage datasets. Following a review of the state-of-the-art in SHM, an autoencoder neural network was selected as the baseline architecture. The principle is to train the autoencoder on simulated structural responses of the healthy state, generated by the calibrated FEM model. Once trained, the network learns to accurately reconstruct the input data corresponding to undamaged conditions. During monitoring, real measurements (e.g. strain profiles, displacement fields, vibration signatures) are processed by the autoencoder. If the reconstruction error exceeds a defined threshold, the data point is flagged as an anomaly, which may indicate the presence of damage. For the steel structural beam, below is presented a table for the damage-identification algorithm that combines strain evolution (local, quasi-static indicators) with modal analysis (global, dynamic indicators) that clearly states the defined thresholds for the algorithm:

Table 5. Defined thresholds for dynamic and static datasets

ID	Indicator	Processing / metric	Threshold / rule (example)	Damage interpretation
D1	Peak strain excursion	max(ε) over load cycle minus baseline	> baseline + 500 με OR > 0.5·yield_strain → alarm	Local yielding / severe local overstress
D2	Residual strain (permanent)	ε_residual = ε_after_unload − ε_baseline	> 100 με and persistent over 3 cycles	Plastic deformation / local damage
D3	Progressive strain increase rate	dε/dt (trend over repeated cycles) or monotonic increase across tests	Increase > 10% over 5 comparable cycles or statistically significant positive trend ($p<0.05$)	Fatigue accumulation or progressive stiffness loss

D5	Fundamental frequency shift	Δf1 = (f1_current − f1_baseline)/f1_baseline ·100%	Δf1 < −2% (beyond environmental bounds) → flag; > −5% → serious	Global stiffness reduction (possible widespread damage)
D6	Higher-mode frequency changes / mode pattern change	Mode shape MAC or Modal Assurance Criterion; Δfn for n>1	MAC < 0.90 with baseline OR consistent Δfn > ±3%	Local damage altering mode shape; boundary change

This approach benefits from several strengths:

- Integration of static and dynamic responses: both deformation (strain/displacement) and vibration data are considered, providing sensitivity to stiffness degradation, crack initiation, and modal frequency shifts.
- Simulation-driven training: synthetic datasets of both healthy and artificially damaged states can be generated from the FEM, enabling controlled evaluation of detection sensitivity and robustness.
- Transferability: by combining simulation data with selected experimental datasets, the approach can address distribution shifts between idealised and real-world measurements, thus reducing false positives.

In practice, the damage detection workflow will operate in three stages:

- Model training with healthy-state FEM data, ensuring a robust baseline of structural behaviour.
- Validation with synthetic damaged scenarios, using FEM to emulate crack propagation, loss of stiffness, or boundary condition changes.
- Deployment on real FOS data, progressively integrating field measurements into the training set to improve generalisation and adapt the algorithm to environmental variability (e.g. temperature, humidity, noise).

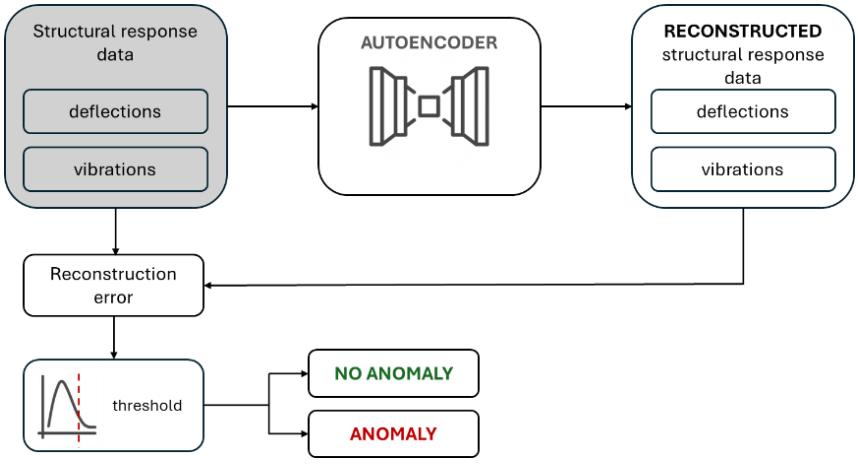

Figure 30. Work scheme for the damage detection algorithm

The final step of the SHM framework developed in Task 2.6 is the damage identification stage, which combines signal processing and AI-based techniques to extract reliable indicators of structural degradation. The methodology leverages both the dynamic response of the structure, obtained from operational modal analysis (OMA), and the static response captured by distributed deformation sensors.

The dynamic component of the algorithm is based on the tracking of natural frequencies and mode shapes identified from FOS and accelerometer data under ambient and controlled excitations. Structural damage or stiffness degradation typically leads to reductions in natural frequencies, particularly in the lower modes, while changes in mode shapes may reveal localised weakening. By establishing a baseline from the calibrated FEM and healthy-state measurements, the algorithm continuously monitors frequency evolution to detect deviations that exceed expected environmental variability (e.g. temperature effects).

```python
import pandas as pd
import numpy as np
import matplotlib.pyplot as plt
from scipy import signal
from reportlab.platypus import SimpleDocTemplate, Paragraph, Spacer, Image
from reportlab.lib.styles import getSampleStyleSheet
from reportlab.lib.pagesizes import A4

# --- Parámetros ---
csv_path = "vibraciones.csv"   # ajusta ruta
fs = 1200.0
target_freq = 93.75
tol = 2.0
win_len_s = 10
win_len = int(win_len_s * fs)
step = win_len
pdf_out = "reporte_modo_93Hz.pdf"

# --- Cargar CSV ---
df = pd.read_csv(csv_path, sep=";")
z = df['Z'].str.replace(",", ".").astype(float).values

# --- Tracking ---
mode_power = []
t_stamps = []
n_windows = (len(z) - win_len) // step

for i in range(n_windows):
    start = i*step
    end = start + win_len
    x_win = z[start:end]
    f_win, Pxx_win = signal.welch(x_win, fs=fs, nperseg=4096)
```

Figure 31. Damage identification algorithm coding

In parallel, the static monitoring provided by the strain sensors (FS62) offers complementary information on deformation trends. By analysing strain distributions along the beam under repeated load cycles, the system can detect anomalies such as localised strain concentration, progressive stiffness loss, or non-linear residual deformations. These tendencies are tracked over time to capture early signs of damage that may not immediately manifest in the global modal parameters.

The combined analysis of frequency shifts (global indicators) and strain tendencies (local indicators) forms the basis of the anomaly detection algorithm. This dual perspective increases robustness: modal frequency changes provide sensitivity to global stiffness degradation, while

strain-based indicators enhance the detection of localised phenomena such as cracks or joint failures. Both datasets feed into the anomaly detection model, which raises alerts when deviations exceed calibrated thresholds.

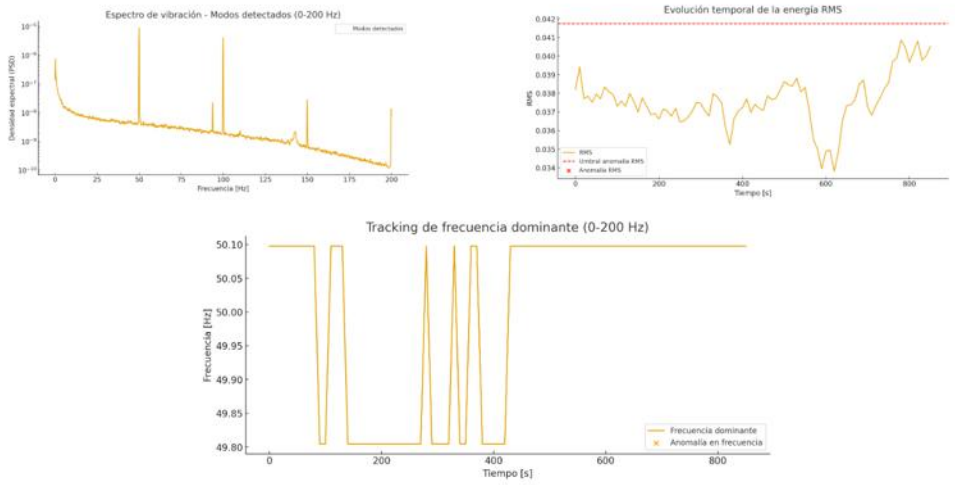

Figure 32. Damage identification algorithm testing execution, related to the vibrational analysis based on RMS acceleration value evolution over time, and shifting of the dominant natural frequency.

This hybrid approach aligns with the broader objectives of SUM4Re by ensuring that reusable structural components are monitored both at the global level (through OMA) and the local level (through strain sensing). Furthermore, the integration of these indicators into the AI-based framework supports future generalisation through Task 3.6 (WP3), where transfer learning techniques will adapt the detection algorithms to new beams and pilot structures.

In summary, the proposed AI-based damage identification methodology represents a scalable, data-driven layer in the SUM4Re SHM framework. It capitalises on FOS precision, FEM-based calibration, and machine learning capabilities to move beyond raw monitoring, providing actionable insights into the structural condition of reused components. This aligns directly with the project's circularity objectives by ensuring that reused elements can be monitored with confidence throughout multiple life cycles.

5. Challenges and limitations

The development of the FOS-based SHM framework in Task 2.6 revealed several technical and methodological challenges (it is stated the related risk of section 4.2):

- Discrepancy between static and dynamic calibration (R9 – Risk-based Assessment Framework). Static tests favoured lower stiffness values (≈136 GPa) while dynamic calibration indicated higher stiffness (≈181 GPa). This divergence is linked to non-ideal boundary conditions and highlights the importance of support modelling for reused elements.
- Sensitivity to boundary conditions (R9 – Risk-based Assessment Framework). Small deviations from the ideal simply supported configuration (cantilever overhangs, partial fixity, or local compliance) had a pronounced influence on dynamic frequencies. Correctly capturing this variability required calibration of support stiffness parameters alongside Young's modulus.
- Sensor installation and bonding (R2, R6, R7 – Risk-based Assessment Framework) – FOS readings proved highly dependent on proper bonding and protection. Surface preparation, adhesive reliability, and environmental protection (humidity, dust, mechanical impact) remain critical to ensuring long-term stability.
- Environmental effects and signal variability (R4, R6 – Risk-based Assessment Framework). Cross-sensitivity to temperature and local noise sources introduced uncertainty in the measurements. Compensation strategies such as reference FOS sensors and filtering algorithms are required.
- Computational demand of FEM calibration. Iterative calibration using genetic algorithms with multiple datasets (static and dynamic) was computationally intensive. While effective, scalability to larger or more complex structures may require more efficient optimisation strategies.
- Representativeness of datasets (R9 – Risk-based Assessment Framework). The calibration relied on a limited number of specimens and loading scenarios. Expanding the reference database, including damaged and aged states, will be essential for transfer learning and generalisation across pilots.
- AI-based detection robustness (R10 – Risk-based Assessment Framework). While the anomaly detection framework shows promise, risks of false positives remain, particularly under environmental variability. Hybrid strategies combining physics-based and AI-based features are needed to improve reliability.

- Use of the calibrated Young's modulus for transfer learning. The compromise modulus of ≈155 GPa, obtained through combined static–dynamic calibration, will serve as a reference value for the training of transfer learning algorithms in Task 3.6 (WP3). A matrix of synthetic scenarios will be generated using this modulus as a baseline, introducing variations in both damage patterns and boundary conditions. This will enable the creation of enriched datasets that capture realistic variability, strengthening the ability of AI models to adapt across structures and pilots.

6. Conclusion

Deliverable D2.6 demonstrates the feasibility and added value of deploying fibre optic sensors (FOS) for the structural health monitoring of reusable steel elements within the SUM4Re framework. Through a combined programme of static and dynamic testing, FEM calibration, and AI-based analysis, the task delivered a traceable methodology for evaluating the condition and reuse potential of structural steel beams.

The work confirms that FOS technology provides high-resolution, multiplexed strain and vibration data with reduced installation effort compared to conventional electrical gauges. The integrated static–dynamic FEM calibration approach successfully reconciled discrepancies between static and dynamic responses, yielding a compromise Young's modulus of ≈155 GPa, consistent with historical steel properties. This calibrated value provides a reliable foundation for further reuse assessment and for training AI models.

A damage identification algorithm was developed, combining operational modal analysis (frequency and mode shape tracking) with deformation trend analysis from FOS strain sensors. This dual-indicator strategy enhances robustness by capturing both global and local signs of degradation. The algorithm is designed to operate in an unsupervised mode, enabling early detection of anomalies without requiring pre-labelled datasets.

Despite these advances, challenges remain in sensor installation robustness, environmental compensation, FEM boundary condition modelling, and dataset generalisation. Addressing these limitations will be essential for scaling the methodology across other pilots and structural typologies.

The findings of Task 2.6 directly support Task 3.6 of WP3, where transfer learning models will be trained on the calibrated datasets to extend anomaly detection capabilities to broader classes of structural elements. Furthermore, integration with WP10 pilot activities ensures that real-world testing informs calibration and validation, while links with WP6 will enable embedding of structural data into circular-BIM platforms and digital product passports.

In conclusion, the methodology developed in D2.6 provides a robust, transferable framework for structural assessment with FOS, combining precision sensing, advanced modelling, and AI-driven analytics. This represents a concrete step toward scalable, digitalised monitoring strategies that underpin circular economy practices in the construction sector.

BIBLIOGRAPHY

[1] Schenato, L. (2017). A review of distributed fibre optic sensors for civil engineering applications. Sensors, 17(4), 946. https://doi.org/10.3390/s17040946

[2] Zhan, Z. (2020). Distributed acoustic sensing turns fiber-optic cables into seismometers. Annual Review of Earth and Planetary Sciences, 48, 293–321. https://doi.org/10.1146/annurev-earth-070619-055104

[3] Min, R., Pinto, A. M., & Marques, C. (2020). Optical fiber sensing for smart civil engineering materials. Sensors, 20(8), 2261. https://doi.org/10.3390/s20082261

[4] Zhang, Y., Sun, L., & Yu, H. (2023). Physics-informed machine learning for structural health monitoring with distributed fiber optic sensing. Mechanical Systems and Signal Processing, 185, 109729. https://doi.org/10.1016/j.ymssp.2022.109729

[5] Min, R., Ortega, B., & Marques, C. (2021). Machine learning for structural health monitoring with fiber optic sensors. *Sensors, 21*(17), 5636. https://doi.org/10.3390/s21175636

[6] Wang, W., Zhang, Y., & Zhang, J. (2022). Deep learning for structural health monitoring: A review of recent trends and challenges. *Engineering Structures, 252*, 113596. https://doi.org/10.1016/j.engstruct.2021.113596

[7] Regulation (EU) No 305/2011 of the European Parliament and of the Council of 9 March 2011 laying down harmonised conditions for the marketing of construction products and repealing Council Directive 89/106/EEC Text with EEA relevance

[8] https://www.codigotecnico.org/

[9] https://www.transportes.gob.es/recursos_mfom/1903100.pdf

[10] https://www.boe.es/buscar/act.php?id=BOE-A-1995-24292

[11] https://www.hbm.com/es/4599/sensores-de-fibra-optica-newlight/?product_type_no=newLight

[12] Ewins DJ. Modal Testing: Theory, Practice and Application. 2nd ed. Research Studies Press; 2000.

[13] Brincker R, Ventura C, Zhang L. Modal identification of output-only systems using frequency domain decomposition. Smart Mater Struct. 2001;10(3):441–445. doi:10.1088/0964-1726/10/3/303

[14] Zhang Y, Aktan AE. Modal identification and damage detection in structures with ambient excitation. J Eng Mech. 1995;121(4):603–614. doi:10.1061/(ASCE)0733-9399(1995)121:4(603)

SUM4Re

Creating materials banks
from digital urban mining

www.sum4re.eu sum4re@uvigo.gal SUM4Re SUM4Re_EU

Funded by the European Union. Views and opinions expressed are however those of the author(s) only and do not necessarily reflect those of the European Union. Neither the European Union nor the granting authority can be held responsible for them.

Funded by the European Union